Fall 2014

Atomization and mixing performance of swirl-venturi lean direct injection

Matthew W. Burkhalter
University of Iowa

ATOMIZATION AND MIXING PERFORMANCE OF SWIRL-VENTURI LEAN DIRECT INJECTION

by

Matthew W. Burkhalter

A thesis submitted in partial fulfillment of the
requirements for the Master of Science
degree in Mechanical Engineering
in the Graduate College of
The University of Iowa

December 2014

Thesis Supervisor: Associate Professor Albert Ratner

Graduate College

The University of Iowa
Iowa City, Iowa

CERTIFICATE OF APPROVAL

_____

MASTER'S THESIS

_____

This is to certify that the Master's thesis of

Matthew W. Burkhalter

has been approved by the Examining Committee
for the thesis requirement for the Master of Science
degree in Mechanical Engineering at the December 2014 graduation.

Thesis Committee: _____
Albert Ratner, Thesis Supervisor

_____
Ching-Long Lin

_____
H.S. Udaykumar

To my family and friends with love.

Keep on beginning and failing. Each time you fail, start all over again, and you will grow stronger until you have accomplished a purpose… not the one you began with perhaps, but one you'll be glad to remember.

-Anne Sullivan Macy

ACKNOWLEDGMENTS

To my parents, Bill and Cindy Burkhalter, for all of their support and love. To Helen Pope for all of your encouragement and patience.

I am very thankful for the technical mentorship I have received over the past few years. Thanks to Dr. Hui Hu at Iowa State for my introduction to laser diagnostics. Many thanks to my current advisor, Dr. Albert Ratner – who has championed my path from the beginning; with application to graduate school, didactic training, and continued support through all my research efforts. While training at NASA Glenn Research Center I was able to have an excellent mentor in Dr. Yolanda Hicks, who gave me detailed guidance and also autonomy to make mistakes and learn by action. To Dr. Sarah Tedder, thank you for your advice and support. To both Dr. Clarence Chang and Dr. Kathy Tacina, I appreciate the many discussions of practice.

I would like to thank Bill Jennings, Steve Struckman and Austin Krebill for help fabricating parts in the machine shop. I would like to thank Jianan Zhang and Daniel Lin for their assistance with data acquisition. Thank you to Kelsey Kaufman, Mohsen Ghamari, Eric Osgood, Yunye Shi, Yan Zhang, Tejasvi Sharma, Majid Emadi, Douglas Karkow and Taleb Salemeh in our research group back at Iowa.

This material is based upon work supported by NASA under Grant No. NNX13AB33A. I would like to thank the Iowa Space Grant Consortium, NASA Glenn Research Center and the University of Iowa.

ABSTRACT

This paper investigated the effects of swirl number and momentum ratio on the atomization and mixing performance of Swirl-Venturi Lean Direct Injection technology. Mie scattering of liquid water, was used to identify the location of water droplets in a cross section of the injector spray. Experiments were performed with three air swirlers with vane angles of 45, 52 and 60 degrees. The swirl number varied from 0.58 to 1.0 and air-to-liquid ratios from 15.8 to 35.6. A transition was observed in the liquid spray distribution for the 52 degree case, which unexpectedly produced twice as much signal than the 45 and 60 degree cases. The main cause of this increased signal may be due to instabilities in the flow when transitioning from low to high swirl states. The results from investigation of swirl number it was found that the spray pattern for is sensitive to swirl intensity. Two flow states were observed for a lower and higher swirl flow as well as a transition state that occurred with the lower swirl state. This work may aid in the specific inquiry of physical mechanisms relating to the effect of flow states on spray distribution. It is found that improved atomization and mixing performance are a result of increase in swirl number.

PUBLIC ABSTRACT

The rising cost of fuels and greater concern for the environment drive efforts in the laboratory to investigate the physics and chemistry of cleaner, more fuel efficient sources of power. Lean combustion has proven to decrease emissions and improve fuel efficiency. In order to achieve the benefits of lean combustion, the method in which fuel and air is mixed becomes critical to the overall performance of the engine. This paper is focused on fuel injection technology for aircraft engines. The objective of this work is to provide qualitative insight into the atomization and mixing process of the Lean Direct Injection. Mie scattering of liquid water was used to identify the location of water droplets in a cross section of the injector spray. High speed photography was used to capture the spray pattern. Experiments were performed with varied the swirl number from 0.58 to 1.0 and air-to-liquid ratios from 15.8 to 35.6 to investigate the effects these have on spray performance. It was found that the spray pattern is sensitive to swirl intensity, that as swirl number increases the spray penetration length decreases and spray pattern moves upstream toward the injector. Both improved atomization and mixing performance are a result of increasing the swirl number. The results of varied air-to-liquid ratio show the mixedness and dispersion of droplets increase with increasing momentum ratio. The results also show decreasing spray penetration length with increasing momentum ratio.

TABLE OF CONTENTS

LIST OF TABLES……ix

LIST OF FIGURES……x

CHAPTER 1 INTRODUCTION ……1
1.1 Background……1
1.2 Objective……6

CHAPTER 2 LITERATURE REVIEW ……5
2.1 Lean Direct Injection……7
2.2 Swirl-Venturi Lean Direct Injection……9
2.3 General Mie Scattering Description……11

CHAPTER 3 EXPERIEMENTAL PROCEDURE……13
3.1 Facility……13
3.1.1 Adaptation of Hardware to Facility……14
3.2 Lean Direct Injection Hardware……15
3.2.1 Fuel Nozzle……15
3.2.2 Air Swirlers……16
3.2.3 Assembly of Fuel Nozzle and Air Swirler……17
3.3 Operation……19
3.3.1 Calibration of Fuel Accumulator……19
3.3.2 Air Supply……20
3.4 Mie Scattering and Imaging……21
3.4.1 Laser System and Optical Assembly……21
3.4.2 Camera, Field of View, and Resolution……22
3.4.3 Procedure and Data Acquisition……23

CHAPTER 4 DATA REDUCTION ……25
4.1 Image Correction……25
4.2 Signal Attenuation……26
4.3 Image Quality……27
4.4 Image Analysis……27
4.5 Statistic Calculations ……28
4.5.1 Mean Calculation……28
4.5.2 RMS Calculation……28
4.6 Comparative Results Calculations……29
4.6.1 Spray Penetration Length……29
4.6.2 Scattered Light Intensity Profiles……30
4.6.3 Spray Cone Angle Calcualtions……30

CHAPTER 5 EFFECT OF SWIRL NUMBER……31
5.1 Effect of Swirl on Atomization and Mixing……31
5.2 Operating Conditions……33

5.3 Swirl Number Results……33
5.3.1 Scattered Light Intensity Profiles……36
5.3.2 Spray Cone Angle Calculations……37
5.4 Comparison with work of Hicks, et al. 2014……38
5.5 Swirl Number Discussion……40

CHAPTER 6 EFFECT OF MOMENTUM RATIO……44
6.1 Effect of Momentum Ratio……44
6.2 Operating Conditions……45
6.3 Mean Results……45
6.4 Momentum Ratio Discussion……54

CHAPTER 7 DISCUSSION ……56

REFERENCES……58

LIST OF TABLES

Table 5.1 Summary of Swirl Cases……..…….33

Table 5.2 Comparison of Test Conditions……39

Table 6.1 Operating Conditions ……...……45

LIST OF FIGURES

Figure 1.1 Emissions relationship with Equivalence Ratio and technologies operating range……3

Figure 1.2 Comparison of fuel injection hardware a.) GE TAPS combustor b.) NASA Multipoint LDI.……4

Figure 1.3 Comparision of NOx emissions for configurations with 45, 52 and 60 degree swirler angles……..…….. 5

Figure 2.1 Swirl-Venturi Lean Direct Injection…….. 9

Figure 2.2 Fuel Distribution inside a lean premixed prevaporization gas turbine at 4 bar……. 12

Figure 3.1 Acoustic Chamber…… 14

Figure 3.2 Components used for testing: simplex fuel nozzle, and air swirlers with: 45 degree, 52 degree, and 60 degree vane angles……..……16

Figure 3.3 Detail of fuel nozzle and air swirler assembly……...…17

Figure 3.4 Test setup……..….18

Figure 3.5 Air flow schematic……....20

Figure 3.6 System for Mie scattering measurement……...21

Figure 3.7 Image of scale to provide magnification factor……..…..22

Figure 3.8 Illustration of test procedure…….……24

Figure 4.1 Image correction a.) Raw image b.) Background image c.) Corrected image…….…..26

Figure 4.2 Threshold process for penetration length calculation…….. 29

Figure 4.3 Example of filtering used for smoothing scattered light profiles……...30

Figure 5.1 Mean and RMS results for varying swirl number……..…34

Figure 5.2 Scattered light profiles of 45, 52, and 60 degree cases…….……37

Figure 5.3 Spray Angle Results……...38

Figure 5.4 Liquid water Mie scattering data……...38

Figure 5.5 Average Mie Scattering Signal (a) 45 degrees, (b) 52.5 degrees, (c) 60 degrees (The flow is bottom to top)……...42

Figure 5.6 Average Velocity Fields (a) 45 degrees, (b) 52.5 degrees, (c) 60 degrees (The flow is top to bottom)…….....42

Figure 5.7 Spray Angle Comparision (a) Example of velocity angle with 60 degree air swirler case, (b) Mie data plotted with mean velocity spray cone angles….43

Figure 6.1 Mean results of cases A1-F1…….47

Figure 6.2 Mean results of cases A2-F2…….49

Figure 6.3 Mean results of cases A3-F3……..…52

Figure 6.4 Spray Penetration Length Results…….55

CHAPTER 1

INTRODUCTION

Most power that we use every day is generated from burning something; whether it be biomass, crude oil, natural gas or coal (Turns, 1996). The rising cost of fuels and greater concern for the environment drive efforts in the laboratory to investigate the physics and chemistry of cleaner, more fuel efficient sources of power. The burning of fuel with an excess of air, or lean combustion, has been shown to reduce harmful emissions as well as increase overall fuel efficiency, a win-win (Dunn-Rankin, 2008). However, there are tradeoffs and challenges associated with this combustion regime; these include lean-blow off, thermo-acoustic instabilities and unburned hydrocarbons (Glassman and Yetter, 2007; Lieuwen and Yang, 2005). In order to achieve the benefits of lean combustion, the method of fuel-air mixing becomes paramount. This paper is focused on aero-engine applications in which various liquid fuel injection strategies exist (Lefebvre, 1999; Khavkin, 2003).

The following is a general description of a conventional combustor in a modern aircraft gas turbine engine. First, liquid fuel is sprayed with air directly into the flame zone, a mixture that is slightly rich. The flame is then stabilized by recirculating air generated by an air swirler with a high swirl number. The flame has a high temperature due to the slightly rich fuel-to-air ratio, this produces high nitrous oxide emissions. Downstream of the primary flame zone, air enters through jets on the walls of the combustor to mix with the hot combustion products. This is to help complete combustion and create a more uniform temperature profile. Current aero-engine manufacturers are improving upon this conventional description with their own proprietary technologies.

The following will look at three aero-engine manufacturer's combustor designs. The General Electric (GE) combustor: Twin Annular Premixing Swirler (TAPS), the Pratt and Whitney: Talon X, and the Rolls Royce: Lean Burning combustor. GE's TAPS combustor consists of a center pilot and outer main; the pilot provides flame stability at low load. Both pilot and main inject a lean fuel mixture into swirling air. For the main injector, fuel is injected out of multiple radial jets along the circumference of the injector (Chang, et al. 2013). For Pratt and Whitney's TALON X combustor, fuel is injected into a rich uniform primary zone using a high shear injector. Then, downstream of the injection, dilution air is rapidly mixed to complete combustion of primary zone products creating an overall lean equivalence ratio (Sturgess, et al. 2005; McKinney, 2007). The Rolls-Royce Lean Burn technology, similar to the TAPS technology, uses concentric main fuel injection and a nested pilot injector for combustion staging (Doerr, 2012).

The ideal liquid fuel injector rapidly mixes fuel and air using a simple means of delivery. To do this, the atomizer must create a fine spray of fuel which is then mixed with incoming air to create a uniform mixture. The atomization and mixing must also occur in relatively short length and time scales, and across a wide operating range. All of these parameters must be addressed while maintaining design simplicity and low production cost. A complex task for the designers of combustion hardware. The three main approaches to aero-engine combustors are: Lean Premixed-Prevaporized (LPP), Lean Direct Injection (LDI), and Rich-burn/ Quick-quench/ Lean-burn (RQL).

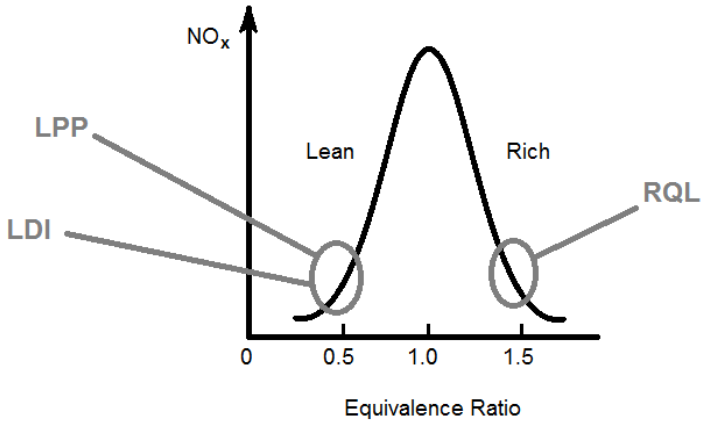

Figure 1.1 Emissions relationship with Equivalence Ratio and technologies operating range

The Lean Premixed Prevaporized (LPP) operates by injecting a lean mixture of fuel upstream of the flame zone in a premixing section which creates a more uniform mixture and very low NOx (Tacina, 1990). First, the fuel nozzle injects liquid fuel and air into a pre-mixing duct or section. In this section, the liquid fuel and air forms a near homogeneous mixture of reactants. The added length of the section offers an opportunity for the atomization process to complete. After exiting this section, the mixture enters the combustion chamber through an air swirler that stabilizes the flame. The flame produces a low temperature flame, which in turn produces low nitrous oxide emissions.

In the Rich Burn/ Quick quench/ Lean Burn (RQL), the fuel and air are injected directly into the flame zone at a highly rich equivalence ratio. The flame is stabilized by a recirculation zone generated by the air swirler. The critical step to this combustor is the rapid injection of air to lower the overall equivalence ratio and complete combustion. There is added length of the chamber to facilitate the quenching and mixing steps. This type of combustor has lower overall NOx

emissions than conventional combustors and higher overall NOx emissions than LPP, however it is more stable over a larger operating range than the LPP (Fu, 2008).

The LDI concept differs from RQL and LPP by injecting a lean ratio of fuel directly into the flame zone at a lean equivalence ratio. [(Tacina,1990), (Hicks and Tacina, 2013)]. This combustor has a lower flame temperature, therefore produces lower nitrous oxide emissions compared to conventional and RQL combustors. The advantages of the LDI combustor compared to the RQL and LPP have been seen in the ability to operate at higher combustor pressures (Tacina, et al. 2008). The LDI has demonstrated low emissions relative to current commercial aircraft technologies [(Marek, et al. 2005), (Tacina, et al. 2012)]. The LDI offers a simple design, shorter combustor length and larger operating range than the LPP (Dewanji, 2012).

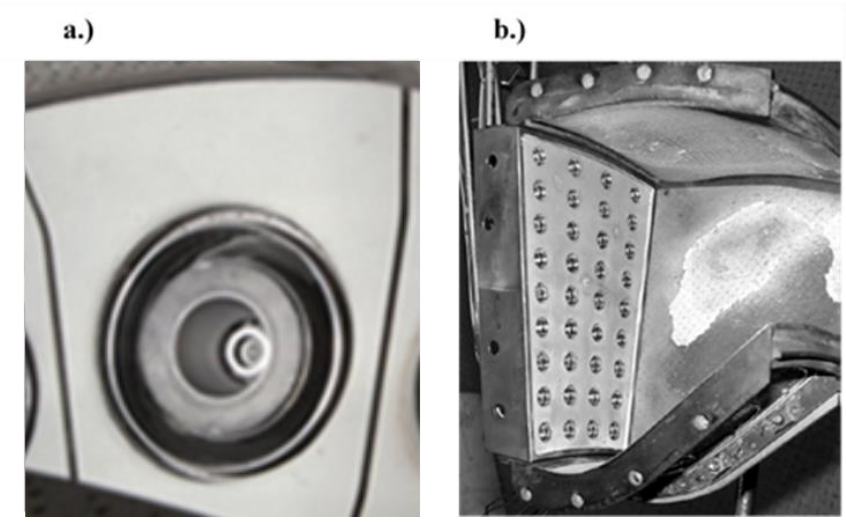

Figure 1.2 Comparison of fuel injection hardware a.) GE TAPS combustor b.) NASA Multipoint LDI

Source: GE: (Chang, et al. 2013), NASA: (Hicks, et al. 2002), Goeke, et al. 2014

Research from NASA, sponsored university programs, and aero-engine subsystem and component suppliers of fuel injectors shows the direction of industry towards multipoint arrays in the next generation combustor. A visual comparison between single point injection and multiple point injection can be seen in Figure 1.2 of the GE TAP's combustor (Chang, et al. 2013) and NASA's 36 point LDI (Hicks, et al. 2002). The benefits from increasing the number of fuel-air mixing sites and decreasing their size has shown to increase mixing performance and decrease NOx emissions (Tacina, 2012). Research efforts in multipoint research are bringing the concept closer to commercialization [(Mansour, 2005); (Chang, et al. 2013); (Goeke, et al. 2014)].

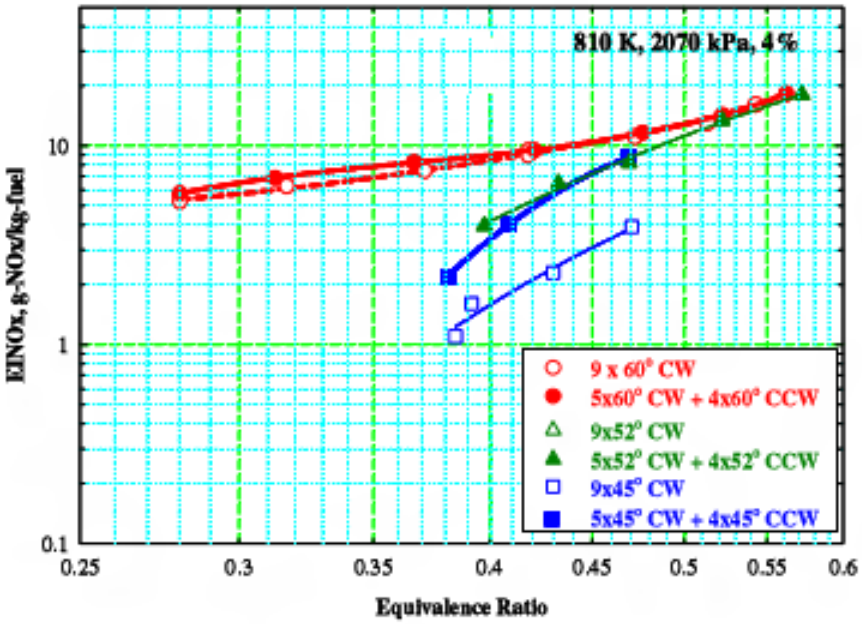

Figure 1.3 Comparision of NOx emissions for configurations with 45, 52, and 60 swirler angles

Source: Tacina, et al. 2005

The work of Tacina and co-workers (2005) were looking into the effect of swirl vane angle on NOx performance. A trend of lower NOx emissions were found for the 45 degree vane angle cases. The 45 degree was also lower than the 52 degree and 60 degree cases. Figure 1.3 shows these trends, with the 52 degree case that is slightly higher in NOx when compared to the mix of 45 degree swirlers. The 60 degree swirlers have the highest NOx production when compared to the 52 and 45 degree cases. In order to investigate the mechanisms that are driving increased NOx production for the 60 degree cases, the problem needs to be dissected; looking into the preparation of fuel and air before combustion and NOx production occur. Before there is NOx production there is vaporization, mixing and atomization of fuel.

1.2 Objective

The objective of this research was to study the effect of swirl vane angle on atomization and mixing. To measure the liquid water distribution of three different air swirlers and the effects of changing momentum ratio on the liquid water distribution. To obtain data in the cold flow field downstream of the Swirl-Venturi Lean Direct Injection hardware and compare with current research efforts at NASA Glenn Research Center. The technique employed in this study was Mie scattering of liquid water, this is used to identify the location of water droplets in a cross section of the injectors hollow spray cone. High speed photography was used to capture the flow physics. The frame rate used was not high enough to freeze the flow; however, the use of statistical methods does provide qualitative picture of the spray topology. The experiments were made to help validate hypotheses of the effects of varying the swirl and momentum ratio on spray performance.

CHAPTER 2

LITERATURE REVIEW

This chapter will provide a brief review of literature that is useful to current research. In section 2.1, prior work relating to Lean Direct Injection and this study is presented with a focus on experimental efforts. In section 2.2, there is a brief explanation of Mie scattering theory which was useful for the present work.

2.1 Lean Direct Injection

The work of Anderson and co-workers (Anderson, 1981) investigated the effect of pressure drop and multi-source injection on NOx performance. Three multi-source airblast fuel injectors, designed by Robert Tacina, were compared against three single source airblast injectors. The multi-source injectors were variations of LPP hardware developed in prior work of Tacina (1978). Anderson found that the single source injectors had generally higher NOx emissions than that of the multisource injectors. It was found that a high sensitivity to injector design on the performance of emissions was also observed. The work of Johnson (1982) investigated the effect of atomization and NOx emissions with and without a venturi. The results from this work show a marked decrease in emissions for cases with a venturi, also shown was a decrease in droplet sizes for venturi cases. It was also mentioned that the effect of the venturi aided the atomization more than that of fuel-air mixing. Locke, et al. (1998) investigated combustion conditions closer to those in realistic systems, appropriately elevated temperatures and pressures using laser-based measurement methods. These tests were brought closer to operation conditions by improvements to optically accessible window cooling. Three fuel injector concepts for aerospace applications were investigated under a broad range of operating conditions. This paper also compares three different diagnostic techniques for spray patternation: PDPA, Mie Scattering and PLIF. Results of

simultaneous Mie Scattering and PLIF imaging show PLIF capturing both liquid fuel and vapor from the pilot and main injector whereas the Mie signal captures only the spray pattern from the pilot. The fine spray and vapors from the main are not picked up. The three measurement techniques were in close agreement and can lead to future quantitative measurement from qualitative images by use of PDPA mass flux reference data.

In his dissertation, Cooper (2000) explored the limitations of high pressure NO-LIF measurements. Discussion of Laser-saturated Florescence (LSF), Laser-induced Florescence (LIF), and Planar Laser-induced Florescence (PLIF) are also made in high temperature and high pressure reacting cases. These reacting cases, with preheated air at pressures of 2-5 atm, were investigated using LIF-NO techniques. The test conditions for the results in this work were 0.165 g/s heptane fuel, 2.78 g/s air, and an air temperature of 375K. A Delavan peanut fuel nozzle was used with flow number of 0.4 along with a 60 degree vane angle air swirler. From point measurements 10 mm downstream of the injector dome, a well-mixed distribution was observed which may be due to recirculation of products from a strong central recirculation zone.

Multipoint testing was investigated (Tacina, et al. 2003) with a 49 point array of fuel injectors and (Tacina, et al. 2004) a 25 point LDI was investigated. Results from these tests gave correlation of NOx emissions with equivalence ratio for each fuel module tested. The results from these investigations were compared against prior multipoint tests and found that 36 point LDI had lowest NOx levels. Marek (2005) performed NOx emission measurements from five different fuel injection configurations burning gaseous hydrogen fuel with air. A test matrix consisted of reduced takeoff, cruise, and approach with equivalence ratios of (0.1 – 0.48). NOx emissions were modeled and correlations found for each geometry. Low NOx emissions for all injectors, a durability concern with high temperature operation, and no flashback or auto-ignition was

observed. The data presented in this work shows NOx concentration has a strong function to axial distance, which helps indicate a small mixing scale for LDI injectors.

2.2 Swirl-Venturi Lean Direct Injection

The LDI has many forms of fuel delivery and air handling to accomplish the goal of rapidly mixing fuel and air into the flame zone. One of the injection concepts is the Swirl-Venturi LDI, which is used in the present work. The Swirl-Venturi consists of an axial air swirler, which has six helical vanes which are set at 45, 52 and 60 degrees for this project. The fuel is injected through a pressure swirl nozzle which creates a hollow spray cone. The venturi is a converging/ diverging section which air and fuel exit the injector as shown in Figure 2.1.

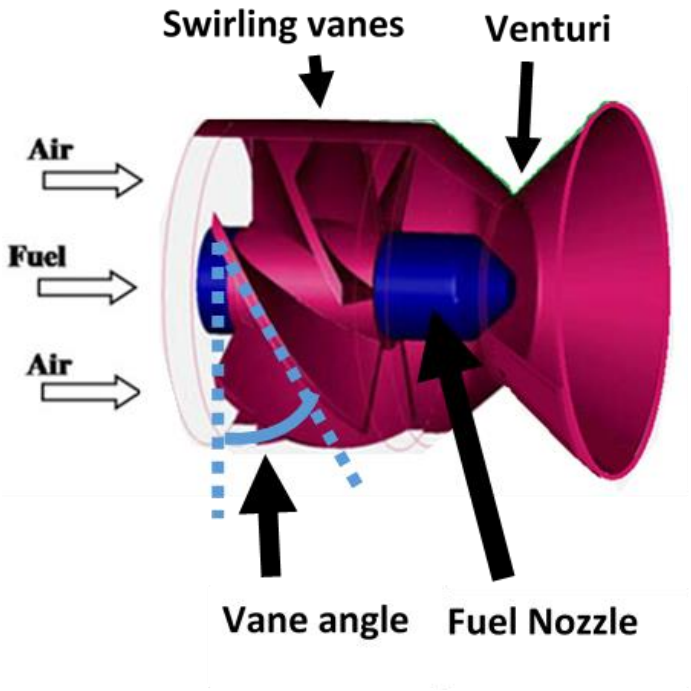

Figure 2.1 Swirl-Venturi Lean Direct Injection

The work of Cai (2005) investigated effects of swirling flow on fuel-air mixing. A reacting case was taken for the single swirler with 60 degree vane angle air swirler, a parker 90 degree fuel nozzle. Jet-A fuel was used with ambient air temperatures and pressures; with a 0.75 equivalence ratio, 0.49 kg/min air, and 0.025 kg/min fuel mass flow rates. Spray visualization was acquired, results shown typical hollow spray cone topology and noted unstable spray distribution patterns. The PDPA technique was used to investigate the liquid spray and gaseous phase velocities. Results show that the gas phase has higher velocities and stronger velocity gradients for reacting cases. Results from the liquid spray, show the Sauter mean diameter (SMD) profiles flatten with increasing axial distance which is due to mixing of the droplet distribution. The results from the volume flux measurements give the reader an indication of how quickly the spray is atomizing and vaporizing downstream of the injector; decreasing a third of the initial volume in 15 mm. Results from the spray velocity measurements provide comparison to gas phase flow and show that smaller droplets match the gas phase flow field closer than that of larger droplets. This paper is highly cited in computational studies as an experimental reference in computational studies [(Dewanji, 2012), (Patel and Menon, 2007), (Knudsen and Pitsch, 2010), and (Iannetti, et al. 2008)].

In work performed by Fu (2008), an investigation of LDI single and multipoint aerodynamics was made. For his dissertation work many test cases were taken, single swirler cases with vane angles of: 40, 45, 50, 55, 60, 65 degrees, as well as confinement effects with varied test section widths 1.0, 1.5, 2.0, and 2.5 inches. Results from confinement had a strong effect on the size of the recirculation zone, the size of the zone increased with increasing cross-section yet turbulent intensity decreased. The effect of Reynolds number was investigated using a 60 degree swirler and 2 inch confinement with Re numbers: 22000, 25000, and 28000. In this study, there were no noticeable effects within this test sample. A reacting test conditions for a single swirler

with 60 degree vane angle and 2 in enclosure, provided insight into the changing nature of flow-field in comparison to the non-reacting cases. For reacting cases, Jet-A fuel was used with ambient air temperatures and pressures, with a 0.75 equivalence ratio (0.49 kg/min air and 0.025 kg/min fuel). The results from these reacting cases show stronger gradients of velocity in the flow. For multipoint testing, cold flow cases of co-rotating and counter swirling arrays of 60 degree vane angle swirlers. Results from co- and counter-swirling cases show similar axial velocity and inverted tangential velocity profiles for the outer swirlers. The effect of a recessed pilot was tested against a baseline with results showing stronger shearing for the central swirler in both co- and counter recessed cases compared to the baseline.

Tacina, et al. (2012) studied five different swirl-venturi SV- LDI configurations each with different sizes and number of injectors. This work isolated the effect of fuel/air mixer size on NOx emission. Inlet air conditions were at pressures of 1.5 MPa and preheated to 840 K, liquid JP8 was used as fuel. In this study it was found that air passage geometry may be more important than fuel/air mixer size below a certain fuel/air mixer size.

2.3 General Mie Scattering Description

Mie scattering theory is a solution to Maxwell's equations which describes the scattering and absorption of incident light upon a sphere (Yushanov, et al. 2013). The solution of radial scattering intensity can be calculated assuming a perfect sphere with an incoming plane wave (Yushanov, et al. 2013). The Mie scattering technique is used for droplets that are much larger than the wavelength of illumination, and Rayleigh scattering is used for droplets smaller than the wavelength (Adam, et al. (2009), Schmidt (2009)). The water spray to be characterized is then illuminated with a laser light sheet, which then scatters off the liquid spheres and this scattered

light is collected with a CMOS camera. The intensity of light scattered is proportional to the size of the droplet (Ng, 2000). The use of Laser Induced Fluorescence (LIF) with Mie scattering can be used to acquire SMD calculations (Mishra, et al. 2014). Using the number density of droplets in a measured region quantitative measurements of fuel concentration can be made (Adam, et al. 2009). Figure 2.2 shows an example of two different techniques measuring the same flow, one measurement is taken using Mie scattering of the liquid fuel distribution, and the second is a laser induced fluorescence of the fuel vapors. This figure highlights that with the use of different techniques one may peel away different layers of the flow. As this papers primary interest is in the initial breakup and mixing of the liquid phase exiting the injector, Mie scattering was used.

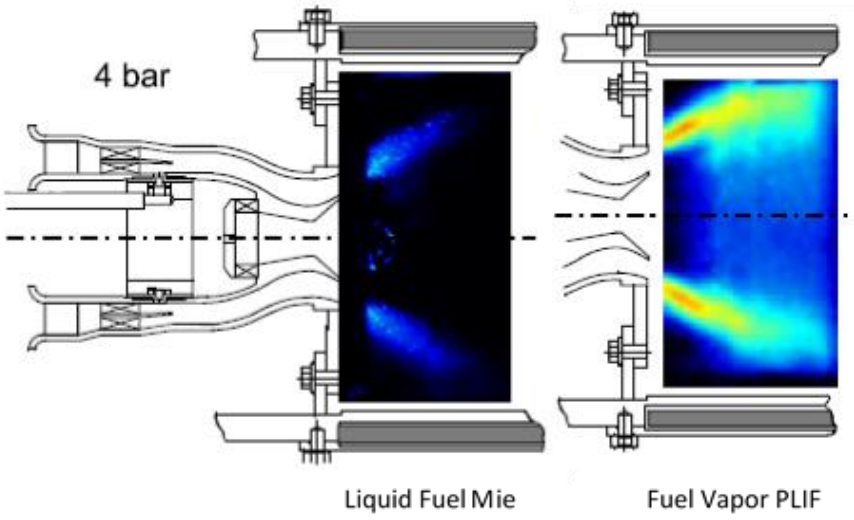

Figure 2.2 Fuel Distribution inside a lean premixed prevaporization gas turbine at 4 bar

Source: R. Fink (2001)

CHAPTER 3

EXPERIMENTAL PROCEDURE

In section 3.1, a description of the facility capabilities and past work is presented. Section 3.2 describes the hardware used in this study and section 3.3 reviews the details of operation. In section 3.4, the methods of imaging and measurement are discussed.

3.1 Facility

Investigation of combustion hardware requires a significant investment in equipment and resources. The Combustion Dynamics Lab at the University of Iowa is well stocked with equipment useful for advanced laser diagnostics: a high power tunable laser, high resolution PLIF camera, high speed camera, pressure and temperature sensors, loud speakers and test chamber suitable for pressurized thermo-acoustic experiments. Metered fuel and air-supply are available by a HASTINGS HFC-203A mass flow meter for the measurement of the air flow to the chamber. There is a vertical section with optically accessible windows for investigation of combustion hardware. Downstream of the test section is four loudspeakers which allow the perturbation of the acoustic field within the chamber. The inner diameter of the chamber is approximately 30 cm with a height of 185 cm, see Figure 3.1. A variable restriction in the exhaust allows operation at chamber pressures of up to 5 atmospheres. This facility has helped advance the study of thermo-acoustic perturbations of the Low Swirl Burner (LSB) with premixed combustion studies (Yun, 2008; Emadi, 2012; Karkow, 2012; Kaufman, 2014). In this study some modification of the facility was made to investigate a liquid spray.

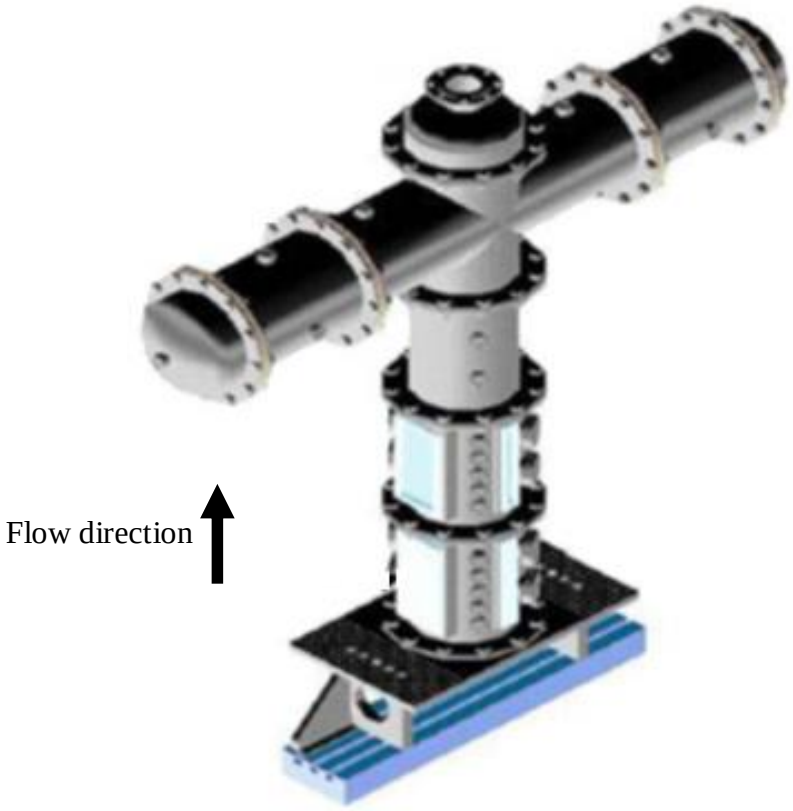

Figure 3.1 Acoustic chamber

3.1.1 Adaption of Hardware to Facility

This section describes measures taken to adapt the facility mentioned which had primarily focused on premixed methane and air combustion of the LSB to a liquid fueled test of LDI hardware. The first measure was the design and fabrication of a fitting to hold the test articles in place. The requirements were to hold the air swirler and fuel nozzle in proper alignment while adapting to the existing test chamber. Two stainless steel blocks were machined down to form the collar. The fuel nozzle was sandwiched between the two pieces which were bolted together to

form a tight seal. The seal between the collar and test chamber was maintained rubber o-ring and bolting the collar to the flange in the chamber.

The second measure to adapt test hardware to the facility was the use of a pressure accumulator. The accumulator was needed to provide the necessary pressure on the liquid for atomization. The fuel nozzle used required a ~50 psid pressure differential from ambient. A compressed nitrogen bottle provided the pressurized gas acting on the liquid. The accumulator used was a Alloy Products Corporation 3.8 L stainless steel pressure vessel with a maximum working pressure of 142 psig at 100 deg F.

3.2 Lean Direct Injection Hardware

The focus of this work is on the atomization and mixing performance of the LDI. This section is intended to provide a visual of what the hardware used in this study looks like and detail on its design. Below is a photograph of the three air swirlers and fuel nozzle used in this study.

3.2.1 Fuel Nozzle

The fuel nozzle used is a pressure driven simplex nozzle, which produces a hollow-cone spray. Chryssakis and co-workers (Chryssakis, et al. 2003) note the benefit of high area to volume ratio for hollow spray cones without large penetration lengths. The fuel nozzle used for this study was a Woodward simplex pressure swirl nozzle with a flow number of 0.7, which produces a hollow spray cone of 85 degrees.

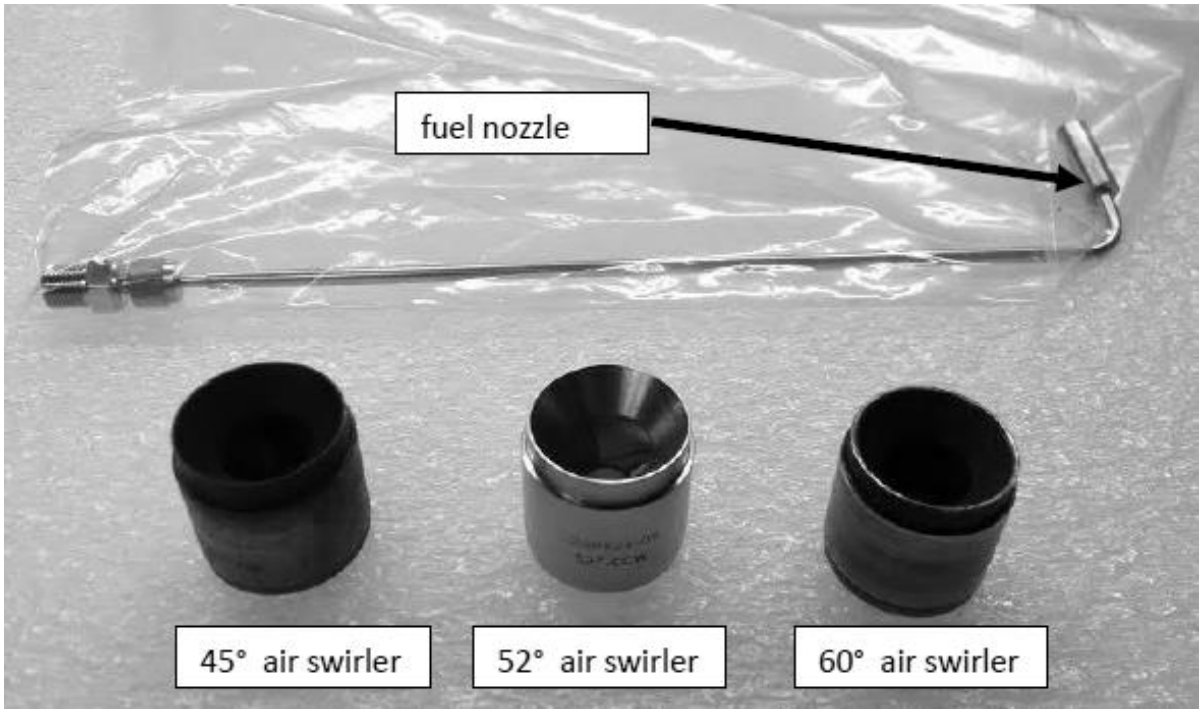

Figure 3.2 Components used for testing: simplex fuel nozzle, and air swirlers with: 45 degree, 52 degree, and 60 degree vane angles

3.2.2 Air Swirlers

The air swirlers used have 6 hexicolidial vanes which are set at 45 CW, 52 CCW, 60 CW. The converging diverging contraction provides a venturi. Johnson (1982) mentions that for a combination of a pressure swirl atomizer and venturi, similar to that used in this work, the Sauter mean diameter of droplets is 30 percent lower than without a venturi. This decrease in drop size can possibly be due to the increase in swirling air velocity at the venturi throat.

Figure 3.3 Detail of fuel nozzle and air swirler assembly

3.2.3 Assembly of Fuel Nozzle and Air Swirler

Figure 3.3 shows the fuel injector assembly, which combines the air swirler and fuel nozzle in a manner that a fully developed spray can be generated and tested. There is a 0.55 inch offset from fuel nozzle tip to exit and a 0.215 inch distance from the venturi throat to the exit, the exit diameter is one inch. The assembly was designed and fabricated to adapt to the existing facility test chamber.

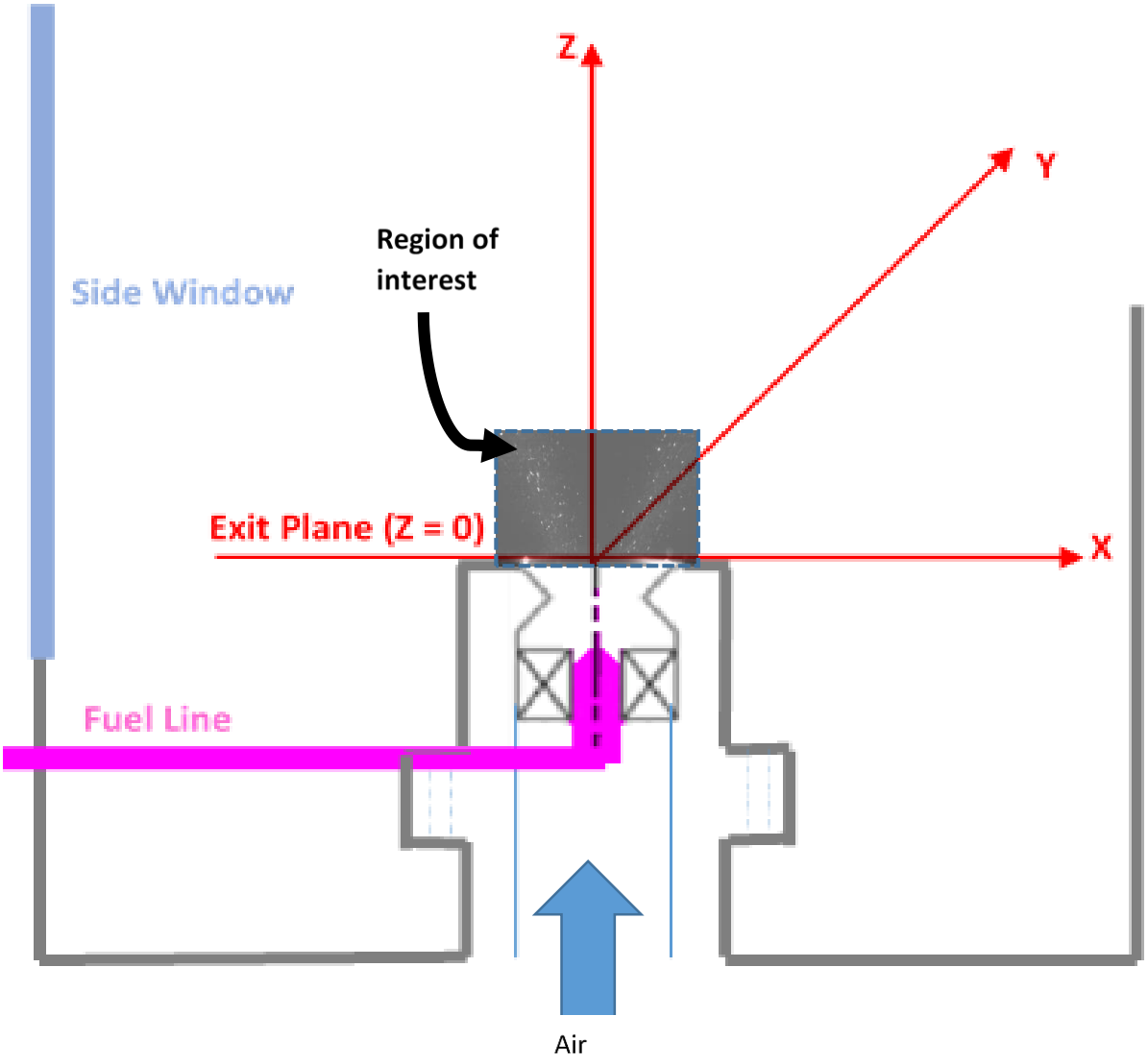

Figure 3.4 Test setup

Figure 3.4 shows the fuel nozzle and air swirler assembly in position with fuel line attached. Showing the air supply flowing through the swirling vanes. This also shows the relative scale of the test hardware to the test chamber, the orientation of the test setup and the size of the region of

interest relative to the test hardware. The laser illumination enters through the side window and images are taken through a window normal to this figure.

3.3 Operation

3.3.1 Calibration of Fuel Accumulator

The water was unmetered and therefore required calibration to quantify the amount of liquid which exits the nozzle at a given pressure. To do this a simple calibration procedure was followed to find a relationship between the internal pressure of the accumulator and the exiting flow rate of the fuel nozzle. The fuel nozzle was setup as it was for the experiments presented in the results section, with the same filters and fittings. A graduated beaker was used to collect the spray. A mass balance was used to measure the mass of the beaker and liquid collected. A timer was used to measure the elapsed time between calibration tests. The calibration consisted of setting the pressure, timing the test from the opening of the valve to closing. The mass was measured for the test run and mass and elapsed time were entered into a spreadsheet. The mass flow rate from five tests for each pressure and each fluid were taken. Pressures of 60, 80, and 100 pounds per square inch were taken and both water and JP-8 were tested. The results found a best fit curve of 0.692 grams per second of water was found for 60 psi, 0.814 grams per second of water was found for 80 psi, and 0.892 grams per second of water was found for 100 psi. The results of the 60 psi calibration test were used for the present work.

The flow number equation was also calculated using the equation:

$$\text{Flow Number} = \frac{\dot{m}}{\sqrt{\Delta P}} \tag{3.1}$$

Where FN is the Flow Number, $\dot{m}$ is the mass flow rate of liquid in [lb/hr] and ΔP is the difference in pressure between that acting on the fluid and atmospheric measured in [psi]. With a ΔP of (60 psi acting on fluid and 14.7 ambient), the $\dot{m}$ for water is 5.494 [lb/hr] from the nozzle. The resulting Flow Number of 0.8162.

3.3.2 Air Supply

The air used in test operation came from rooftop compressors that was then fed into a HASTINGS HFC-203A mass flow meter before entering the test hardware. This flow controller was used to set the volumetric flow rate of air for experimental test points. The accuracy of measurement was recorded within +/- 10 slpm.

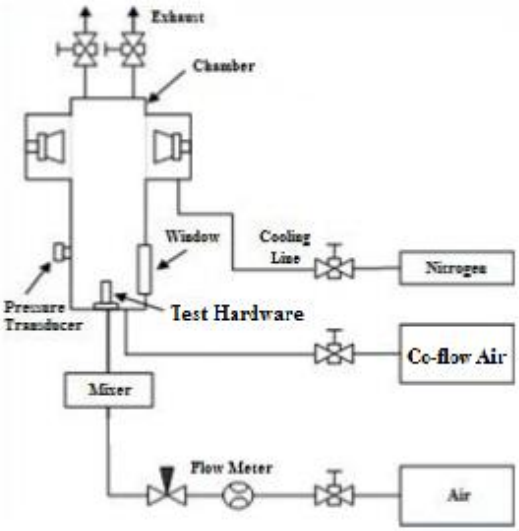

Figure 3.5 Air flow schematic

3.4 Mie scattering and Imaging

3.4.1 Laser System and Optical Assembly

The laser system used for testing consisted of a laser and optical train arranged to create a laser sheet. The laser used was a Laserglow Technologies LRS 532 nm 5W continuous wave laser. The laser sheet cut a section of the spray and provided the necessary illumination to gain enough scattering signal from the liquid water spray. The measured beam strength before the optical train was 2.6 W. The laser sheet height was approximately 2 cm and a thickness of 1 millimeter. The estimated power density of illumination is approximately 12.5 W/ cm^3.

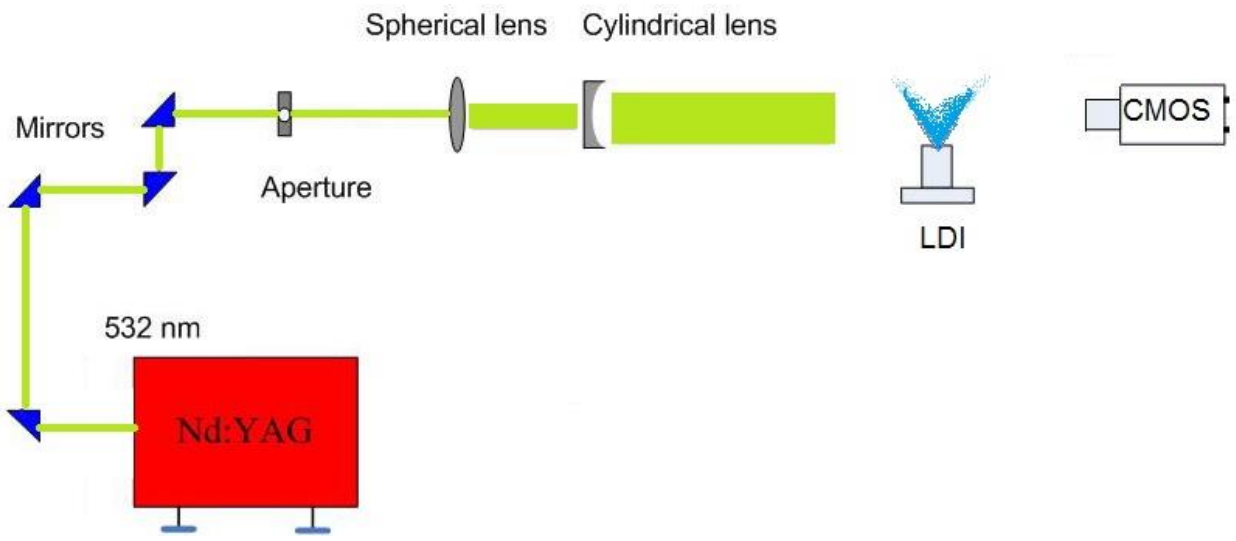

Figure 3.6 System for Mie scattering measurement

3.4.2 Camera, Field of View, and Resolution

A balance of frame rate, laser intensity, and flow rate exist in order to acquire a strong signal to noise. The frame rate used for this study was 1,050 hertz and the field of view was 2.7 cm by 3 cm. The tests performed are at the envelope of our facility in terms of airflow rates approaching 30 grams per second of air or 40 meters per second. At these conditions the signal decreased and greater laser power was required to compensate for the increased frame rate and decreased exposure. Many lessons were learned through iterative testing of acquisition settings to arrive at the appropriate balance of laser power, exposure, and framerate.

The images acquired for all results presented were taken with the same aperture and exposure, the laser power was also fixed. The camera used for testing was an IDT X-Stream high-speed camera. The magnification of images taken was found to be 0.04429 mm per pixel.

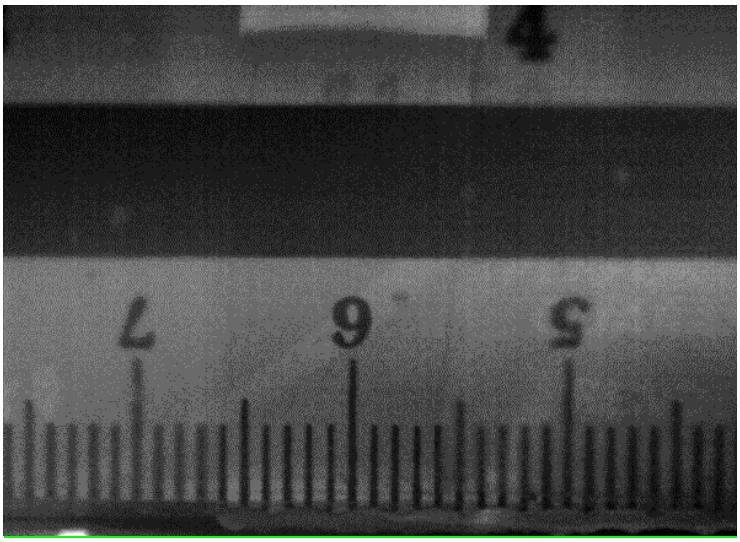

Figure 3.7 Image of scale to provide magnification factor

3.4.3 Procedure and Data Acquisition

The following is an outline of the procedures taken in conducting the spray performance experiments.

1. Place hardware in chamber

   For a given test configuration place air swirler into collar inside of test chamber. Bolt and secure.

2. Laser warm up

   Turn on laser. Optic alignment for maximum signal. Measure laser power. Record.

3. Prepare Air supply

   Open valves supplying air to test chamber. Turn on flow controller.

4. Prepare fuel supply

   Open valve to compressed nitrogen tank. Set pressure to accumulator

   Read pressure on both bottle and accumulator gauges.

5. Prepare imaging

   Turn on camera. Focus camera to card and laser. Set exposure and frame rate.

6. Turn on spray

   Open valve to accumulator.

7. Take data.

   Turn off lights to the room. Turn on laser (open shutter)

   Acquire images

   Close laser shutter

   Close valve to accumulator

   Turn on lights to room.

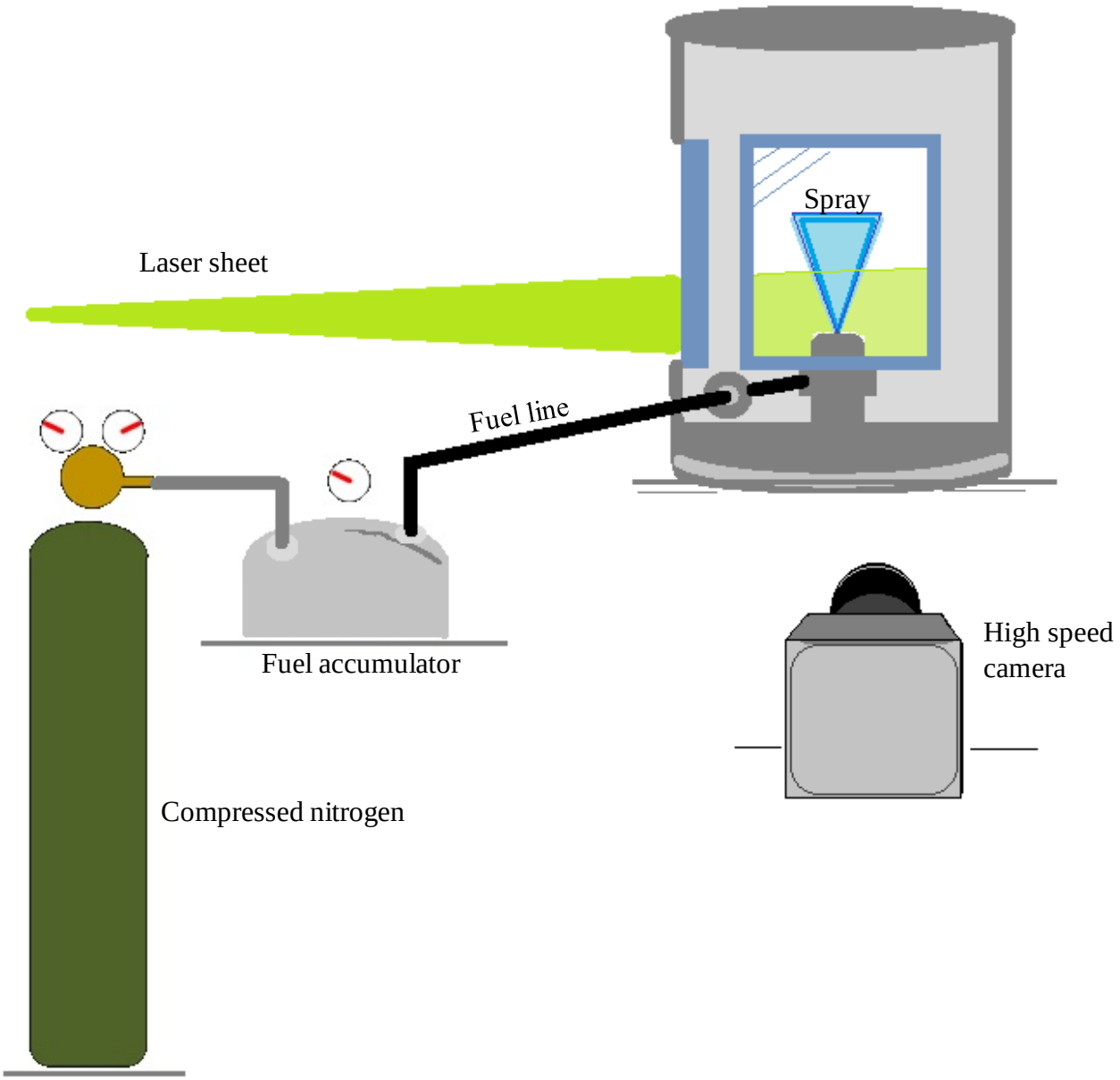

Figure 3.8 Illustration of test procedure

CHAPTER 4

DATA REDUCTION

In section 4.1, the methods used to subtract background noise from raw images are presented. In section 4.2, the quality of the signal attenuation is discussed. In section 4.3 image quality discussed and in section 4.4, image analysis. In section 4.5 the methods for calculating the mean and RMS statistics are shown. In section 4.6, the methods for penetration length, calculating the spray cone angle and spray distribution are presented.

4.1 Image Correction

The methods for preparing the images for analysis are explained. To remove noise from the raw data image, the raw data images were subtracted from the average background to obtain a corrected image. The goal of these corrections is to reduce the intrinsic noise of the camera and scattered light from the illumination source. Figure 4.1 shows a typical image correction process with raw instantaneous image, average background image and corrected data image. The corrected data image was the difference of the instantaneous raw image from the averaged background image. The corrected image is then used in ensemble averaging as well as scattered light intensity profiles and contour plots of mean statistics. Further discussion of sources of noise and signal quality will be discussed in the next two sections. The average background is taken from 1,000 images of the region of interest with the laser sheet active and without air or liquid water flowing. This background is used to provide a look into the ambient noise associated with data collection.

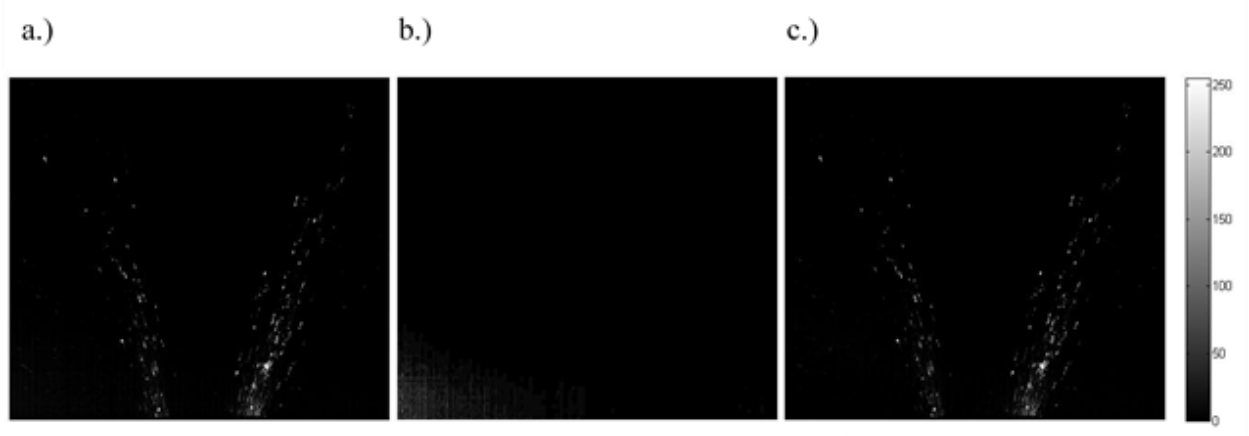

Figure 4.1 Image correction a.) Raw image b.) Background image c.) Corrected image

4.2 Signal Attenuation

The observed scattered light is stronger on the incoming side of the laser sheet. As the laser sheet enters the spray cone, layers of droplets attenuate the signal for the subsequent side of the spray cone. This is common to laser diagnostics and can be corrected by bi-directional illumination (Charalampus and Hardalupas, 2014) as well as modulated illumination such as structured light (Mishra, et al. 2013). Laser attenuation also varies from test condition to test condition as different flow conditions create a different field of attenuation for the laser to traverse. In the results signal attenuation is observed to be 16%. The signal attenuation is related to the number density of water droplets in the flow, the area of incident illumination and the path length which the laser sheet cuts through the spray. The expression that describes the decrease in energy density of the laser sheet, Beer's Law, is the following:

$$\frac{I}{I_0} = e^{-\sigma NL} \tag{4.1}$$

Where σ, is the cross section of the laser sheet [cm^2], N is the number density [cm^{-3}], and L is the path length [cm]. If the region of interest were homogeneous a subtraction of the flat-field laser signal would be sufficient for correction. Since the data field is stratified a line integration would be necessary for image correction. The laser attenuation can be assumed to pass through layers of signal attenuation, discussed as layers of an onion in analysis of the signal attenuation coefficient (Brown, et al. 2002). This layered attenuation can be seen further in (Wellander, et al. 2011) and (Charalampus and Hardalupas, 2014).

4.3 Image Quality

The signal intensity from a droplet is read at 50 units and the dark region is on average 5 out of 255 units. The on-chip noise of the camera is noticeable in the ensemble averaged mean and rms results and provides an exaggerated cross-hatching effect. The quality of the laser sheet can create striations in the illuminated area of interest which is also observed. The secondary scattering in the region of interest can give reduced image contrast (Brown, et al. 2002; Berrocal, et al. 2008).

4.4 Image Analysis

In this section brief discussion is made to the interpretation of results relating to the atomization and mixing efficiency of the fuel injectors tested. Atomization being the reduction in liquid droplet size to vapors and mixing being the quality of bringing two or more different states into a homogenous state. A figure demonstrates the differences between atomization and mixing, an image may show poor mixing but excellent atomization or likewise excellent mixing and poor atomization. The color bar used to scale the images presented in the results has gradient of colors

which range from blue to white. In the images blue represents the lowest pixel value, while white represents the highest pixel value. The more liquid the brighter and therefore stronger signal..

4.5 Statistic Calculations

4.5.1 Mean Calculation

To provide qualitative inference on the performance of sprays mean and rms statistics were used. The mean statistics help show the nature of spray topology for a given test condition. The profiles of spray distribution and spray cone angle are calculated using the mean image. The ensemble average of images acquired was calculated using the following form:

$$\bar{x} = \frac{\sum x_i}{n} \tag{4.2}$$

Where $\bar{x}$ is the mean image, x_i is the corrected data image and n is the number of images taken. A total of 1,000 corrected images are used to calculate the mean image.

4.5.2 RMS Calculation

The procedure to calculate the RMS for the image begins with calculating the mean square of the image:

$$\overline{x^2} = \frac{\sum(\bar{x}-x_i)^2}{n} \tag{4.3}$$

Where $\overline{x^2}$ is the mean square of the image, $\bar{x}$ is the mean image and x_i is the corrected data image. The above expression is multiplied by the half power to arrive at root mean square:

$$x_{rms} = \sqrt{\frac{\sum(\bar{x}-x_i)^2}{n}} \tag{4.4}$$

4.6 Comparative Results Calculations

4.6.1 Spray Penetration Length

The penetration length was found using a method similar to Siebers (1998), where a threshold was taken at a percentage of the maximum scattered light. Thresholds were taken at approximately 3% of the maximum signal. First a threshold of the mean image was taken at 3% of maximum intensity. Then the distance was measured to the farthest point downstream, and lastly the distance was converted from pixels to mm using the magnification factor mentioned previously of 0.04429 pixels per mm. Figure 4.2 shows a sample of an image used in this process.

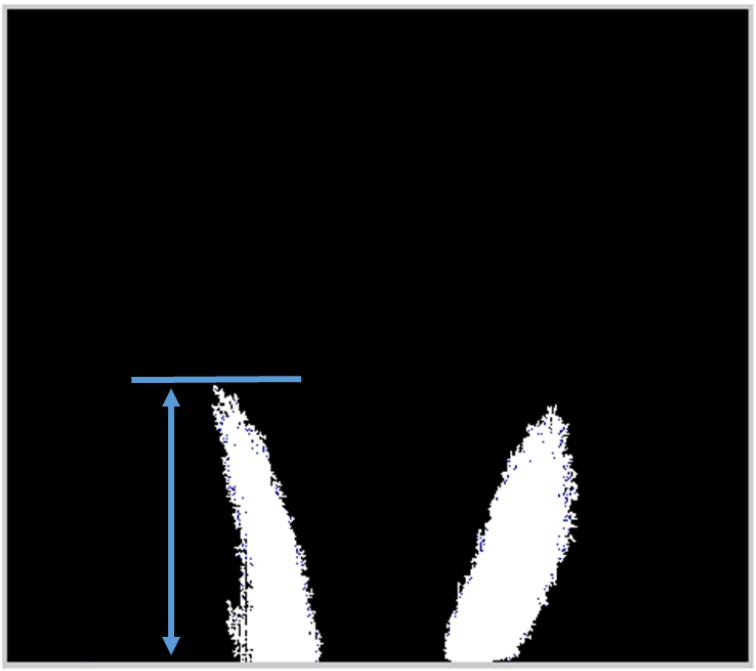

Figure 4.2 Threshold process for penetration length calculation

4.6.2 Scattered Light Intensity Profiles

The distribution or spray profile is taken by plotting the scattered light intensities along a line which is a fixed axial distance from the spray dome. To smoothen the signal a moving average was used, this helped reduce uncertainty in later calculations which required peak-to-peak distances. An intrinsic function which applies a moving average to a time series, a lowpass filter, for the results shown the filter coefficients equal to the reciprocal of the span which was set to 21. A survey of spans was used to find the minimum span which allowed the goal of a clearly distinguishable peak.

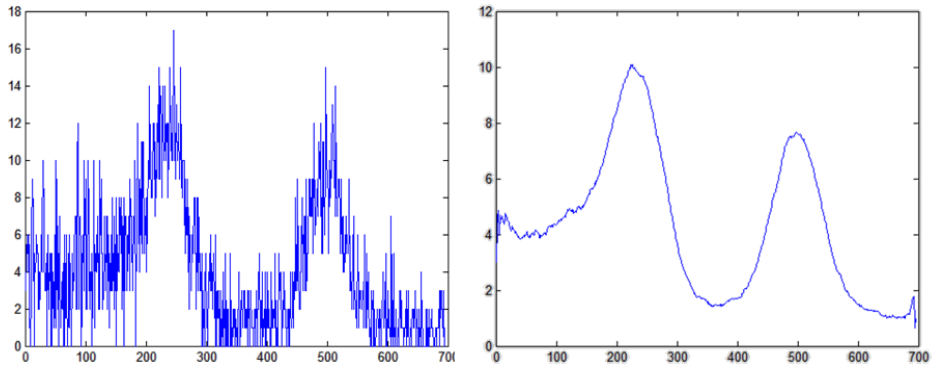

Figure 4.3 Example of filtering used for smoothing scattered light profiles

4.6.3 Spray Cone Angle Calculations

The procedure for approximating the spray cone angle is adapted from that of (Locke, et al. 1998). Which used the change in fuel ring diameter along with the axial displacement between measurements for a simple geometric calculation. For the results presented, the change in peak-to-peak distance of scattered light intensity is used instead of fuel ring diameter. The spray angle is then equal to twice the tangent of the change in peak-to-peak distance over the change in height between measurements of scattered light intensity profiles.

CHAPTER 5

EFFECT OF SWIRL NUMBER

In section 5.1 the initial question of the effects of swirl on the atomization and mixing performance is posed. In section 5.2, early testing of varying vane angle is presented and compared with current literature. In section 5.3, the results of the Mie scattering of liquid water of three different swirl numbers is presented. In section 5.4, the results for the 60 degree air swirler are compared with work of Hicks, et al. (2014). In section 5.5, a discussion of the results is made.

5.1 Effect of Swirl on Atomization and Mixing

The intent of this work is to provide qualitative insight into the nature of atomization performance with varying swirl intensities. Swirling flows have been well studied in combustion and provide an excellent means for flame stabilization in gas turbine and industrial application. Yang highlighted some characteristic features of swirling flow fields: corner recirculation zones, strong shear layers, precessing vortex cores, vortex breakdown and central recirculation zones. Recirculation of products back into the flame zone provides a continual source of heat helps the flame stay lit (Feikema, et al. 1990). In work by (Liang and Maxworthy, 2005) provide a detailed investigation of the underlying fluid dynamic phenomena of swirling jets and the instabilities that lead to vortex breakdown.

In work from (Syred and Beer, 1974), there are two primary methods of swirl generation, the use of guide vanes in axial tubes and tangential entry of fluid stream into duct. The use of guide vanes was used in this study to impart angular momentum on the air flow. (Syred and Beer, 1974) also gave a definition of swirl as a ratio of angular to linear momentum of fluid flowing out the injector, as follows:

$$G_{\Phi} = \int_0^R (Wr)\rho U 2\pi dr \tag{5.1}$$

$$G_x = \int_0^R U\rho U 2\pi dr + \int P \cdot 2\pi r dr \tag{5.2}$$

Where G_{Φ} is the axial flux of angular momentum and G_x is the axial flux of linear momentum. In this expression. W, is the tangential component of velocity and U, is the axial component of velocity. The swirl number, S, is therefore:

$$S = \frac{2\, G_{\Phi}}{G_x D_e} \tag{5.3}$$

Where D_e is the diameter of the exit. Another formula of swirl number used in recent work of Yoon et al 2012, begins as follows:

$$S = \frac{\int \rho r V_{\theta}\, (\mathbf{V} \cdot \mathrm{d}\, \mathbf{A})}{\bar{r} \int \rho V_x\, (\mathbf{V} \cdot \mathrm{d}\, \mathbf{A})} \tag{5.4}$$

Starting with a similar formulation to Syred and Beer as a ratio of angular to axial momentum by definition, then using a geometric derivation from Fu (2008):

$$S = \frac{R_2^2 + R_1^2}{2R_2^2} \tan(\theta_m) \tag{5.5}$$

Where R_1 is the radius of the fuel nozzle and R_2 is the radius of the swirler vane and θ_m is the vane angle (of the helical axial-vaned swirler).

5.2 Operating Conditions

The operating conditions used for investigation into effect of swirl are shown in table x. The mass flow of air at 1.57×10^{-2} kg/s and liquid water at 6.92×10^{-4} kg/s were fixed for all three test cases. Table 5.1 shows a summary of relevant parameters for the three test cases:

Table 5.1 Summary of Swirl Cases

Case	Vane angle	Swirl pattern	Swirl Number	Reynolds Number	Air Velocity
1	45	Clockwise	0.58	12,000	8.65 m/s
2	52	Counter –clockwise	0.74	12,000	8.65 m/s
3	60	Clockwise	1.0	12,000	8.65 m/s

5.3 Swirl Number Results

The mean and RMS results are presented in Figure 5.1 showing the three different test cases mentioned above. The results help show both the average spray shape and variation from that average. All three cases were taken at the same operating condition with the same mass of air and the same mass of water. This means that the same amount of liquid is entering the frame for each case. The image acquisition settings were used with the same laser power density, frame rate, exposure, and focal length. The only variation between the three cases was the swirler hardware used. Case 1: had a 45 degree vane angle oriented in the clockwise direction. Case 2: had a 52 degree vane angle oriented in the counter-clockwise direction. Case 3: had a 60 degree vane angle oriented in the clockwise direction.

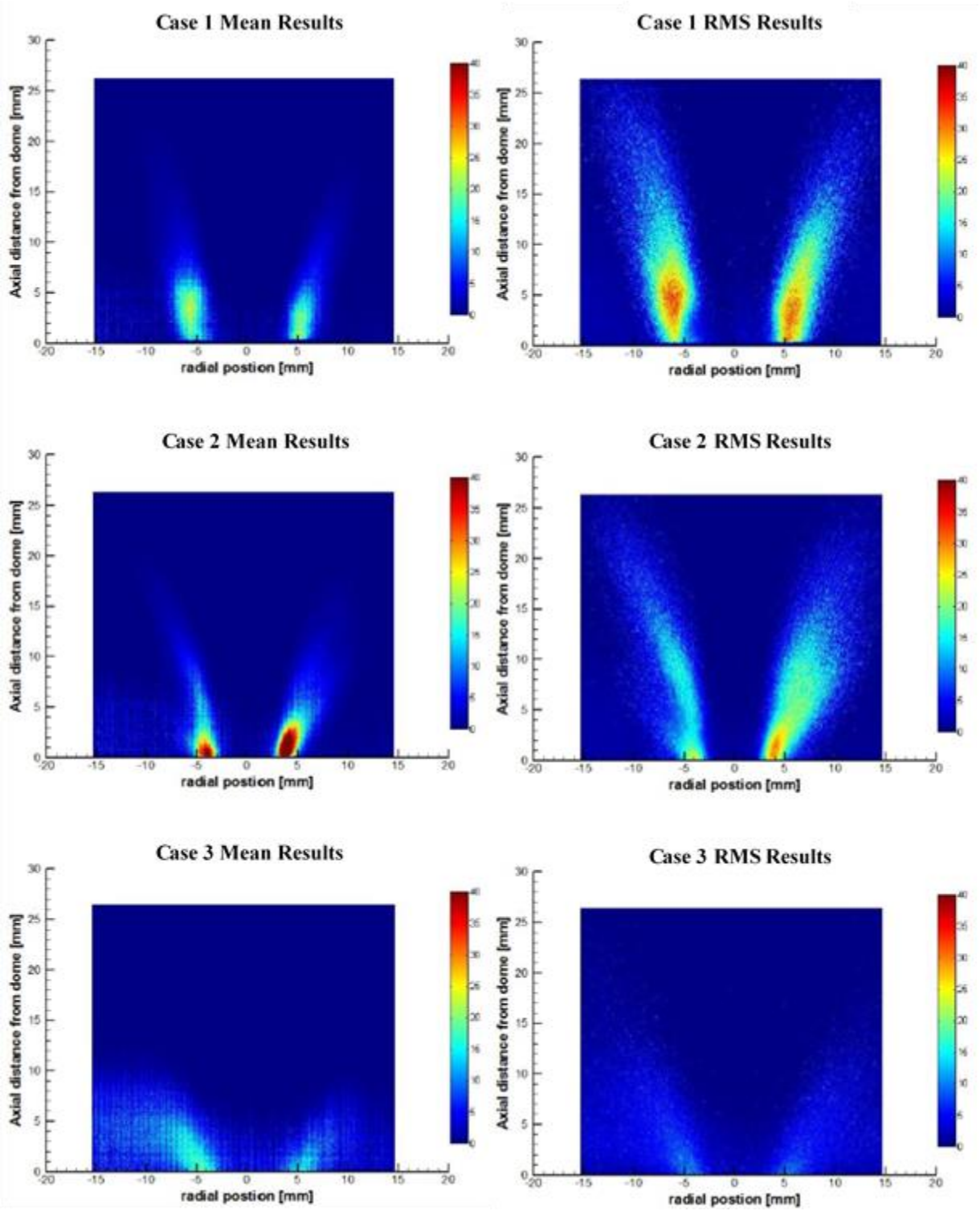

Figure 5.1 Mean and RMS results for varying swirl number

From the results it can be seen that Case 1 and 2 have a similar spray penetration lengths. Case 3 has a shorter penetration length compared to the other cases, roughly a half of cases 1 and 2. In case 1 with a threshold of 3%, the length was approximately 22 mm downstream of the frame. Case 2 the penetration length was 20 mm downstream of the frame at a 3% threshold. In Case 3 the penetration length was 11 mm downstream of the frame at a 3% threshold. The shorter penetration length of case 3 is an indication of good atomization, both the smaller and larger droplets do not extend far downstream of the injector dome. Cases 1 and 2 on the other hand have the bulk of the liquid spray penetrating to roughly 10 mm downstream and then smaller drops extending further to 20 mm. The longer penetration lengths of cases 1 and 2 are likely due to the greater axial momentum of airflow at the injector exit. A possible cause for the similarity in penetration lengths of cases 1 and 2 maybe due to the low quality of atomization in case 2. Case 2 could have otherwise produced a shorter length than case 1, but as there is greater liquid present near the exit, that liquid then required further breakup downstream resulting in a longer penetration length.

The signal intensity of the results is a qualitative measure of how much liquid is present in the frame, as the signal increases the amount of droplets and droplet size increases. Conversely the signal intensity decreases as the drop size decreases. Of the three cases presented, case 3 has the finest atomization performance noted by lower signal. Case 2 has considerably more liquid at the exit which is an indication of low atomization efficiency. The results from case 1 show greater better atomization than case 2 but worse than case 3. The cases with clockwise vane orientation seem to perform better than that of the counter-clockwise case, case 2 in terms of atomization. This may be due to an effective reduction in angular momentum as two flows interact.

The mixing performance of the three cases can be assessed qualitatively by how well the liquid spray is dispersed with incoming air. Case 3 also shows a fairly well distributed spray, the strong tangential flow is likely entraining fresh air and mixing in recirculation zones at the corners of the frame. Case 1 and 2 have comparatively poor mixing with that of case 3, the liquid spray cone exits the injector and travels downstream with minimal indication of mixing in the mean results. The RMS results for cases 1 and 2 however do show mixing, by showing the fluctuation from the mean of liquid water present.

The RMS data shows scalar, liquid water, signal fluctuations from mean values. This data can be useful in measuring the mixedness of the cases presented. In case 1 there is a lot of variability from the mean spray pattern. Both the right and left lobes of the spray cone have a larger spread angle showing that the possible trajectory of the spray has a great deal of variability between frames. In case 2 there is less variability intensity than case 1, though the fluctuations do cover a larger area than the mean data. Case 3 does not show great variation from the mean indicating that the mean results are capturing the spray pattern well.

5.3.1 Scattered Light Intensity Profiles

In a similar manner as Cooper and Laurendeau (2000), Mie scattering data taken at a given axial distance gives a radial profile of the scattered light intensity. As the scattered light intensity is related to the amount of liquid present, the profile serves an analog to the radial spray distribution of droplets. From the Figure 5.2 the three cases are plotted at the same axial distance. This figure highlights variation in signal quality and spray pattern between cases. Case 1 has a similar peak intensity as case 3. Case 2 has a very strong signal with scattered light intensity more than twice that of cases 1 and 3. This strong signal is likely due to larger water droplets, and indication of poor atomization. The shapes of the profiles also give indication to how dispersed the spray is at

the particular axial position. Case 2 has narrow peaks, showing that the light is scattered off densely packet drops of liquid whereas in cases 1 and 3 the profiles are radially spread out. Between cases 1 and 3, case 3 is slightly flatter and therefore a more dispersed spray pattern.

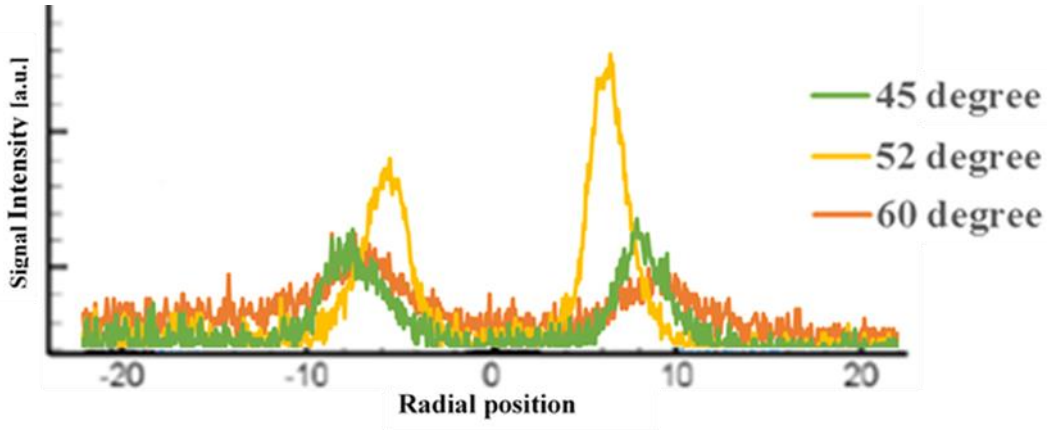

Figure 5.2 Scattered light profiles of 45, 52 and 60 degree cases

5.3.2 Spray Cone Angle Calculations

Measurements of the spray cone angle were made from the mean scattering data using the procedure outlined in section 4.6. Case 1 had a measured angle of 29 degrees, case 2 had a measured angle of 39 degrees, and case 3 had a spray angle measured to be 98 degrees. The narrow angle of the sprays in cases 1 and 2 are likely due to greater axial momentum of the air flow compared to case 3. A nonlinear behavior is noticeable when plotting spray cone angle versus the air swirler vane angle, see Figure 5.3. The 45 degree and 52 degree air swirler produce spray cone angles that are within 10 degrees of each other. Then the 60 degree air swirler creates a much wider spray cone which is more than double that of the 45 and 52 degree air swirlers.

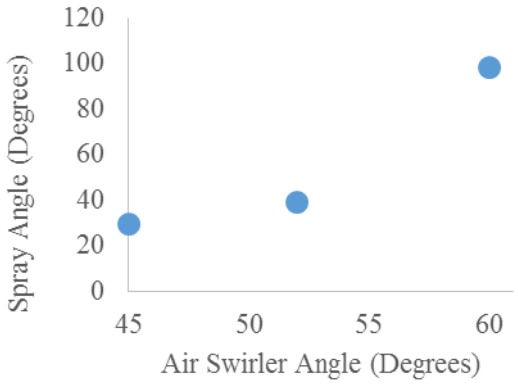

Figure 5.3 Spray Angle Results

5.4 Comparison with work of Hicks, et al. 2014

Some comparison of results can be made with the recent work of Hicks, et al. (2014). In this work, laser scatter was used to identify locations of liquid spray in a similar fashion as in the results in this paper. For this work preheated air was used with co-flow air, the flow direction was downward with gravity. A 30 kHz frame rate compared the frame rate used in this work of 1,050 Hz. Liquid water was used Figure 5.3 shows results from Hicks with a 60 degree air swirler.

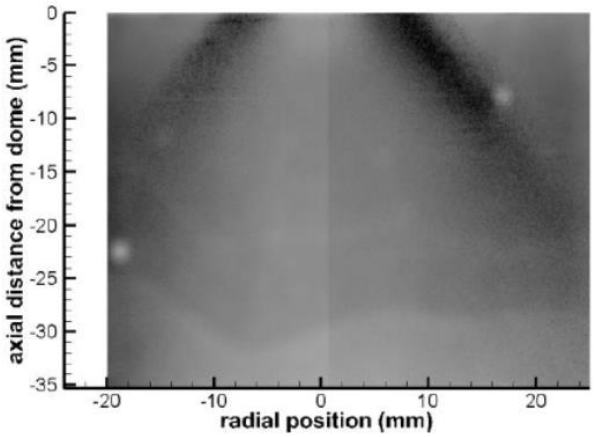

Figure 5.4 Liquid water Mie scattering data

Source: Hicks, et al. 2014

For Hicks, et al. (2014) the spray cone captured by imaging extends farther downstream with a penetration length of 20 mm compared to 10 mm for the work presented in this paper. Hicks measured a spray angle of approximately 75 degrees and the present work the spray angle was found to be 98 degrees. Some of the reasons for differences in penetration length and spray angle may be due to differences in operating condition. Table 5.2 highlights some of the differences in operating conditions with air temperature and pressure, mass flow rate and velocity. The co-flowing air may aid in stretching the spray axially with the flow. In the work presented it appears that in the absence of co-flowing air the spray is free to spread outward and the strong angular momentum brings the spray out into the corners of the frame.

Table 5.2 Comparison of Test Conditions

Hicks, et al. (2014)	Present work
T_{air} = 700 K, P_{air} = 517.1 kPa	T_{air} = 297 K, P_{air} = 101.3 kPa
mass flow air = 0.179 kg/s (including co-flow air)	mass flow air = 0.0158 kg/s
mass flow water = 1.085 g/s	mass flow water = 0.692 g/s
Ref velocity = 15.2 m/s	Ref velocity = 8.65 m/s

Another difference in spray pattern may be effected by the flow direction of the spray. In the work presented, the flow direction is upward against gravity. This may affect the trajectories of the droplets pulling them downward, likewise for Hicks the spray may also be pulled downward with the spray pattern closing in at the liquid breakup length. This may cause a slightly narrower spray cone than the work presented as the spray could be pulled open.

5.5 Swirl Number Discussion

The results of the Mie scattering data show a transition in the liquid distribution between cases 1 and 3. The change in liquid distribution between the 0.58 and the 1.0 swirl cases may be caused by a transition in the flowfield. The transition from low swirl to high swirl has been well documented in literature [Syred and Beer (1974), Vanierschot and Van den Bulck (2007), and Falese, et al. (2014)]. There has also been a great deal of computational and experimental work highlighting the flowfield of the Swirl-Venturi LDI, of these the experimental work of Fu (2008) and Tedder, et al. (2014) will be used for discussion.

The spray shows similar penetration length and spray cone angle for cases 1 and 2. Case 2 has a much stronger signal than cases 1 and 3. Case 3 has the most dispersed flow with a high degree of mixing and a penetration length half that of cases 1 and 2. There is a marked shift in the spray pattern that occurs between case 2 and 3. The transition may also be occurring close to the swirl number of case 2. The higher amount of laser scatter of this case may relate to this flow transition.

The transition of the spray distribution seems to occur about case 2, which has a swirl number of ~0.74. Syred and Beer (1974) discuss the occurrence of vortex breakdown as a function of Reynolds number and swirl number, and that this occurs for flows with a swirl number greater than 0.6 and Reynolds number from 2,000 to 18,000. Case 2 is in this range. Case 1 is in one flow state and Case 3 is in another. The work of Vanierschot and Van den Bulck (2007) experimentally investigated and classified different swirling flow states. Four different flow states were found and hysteresis was also observed. Falese, et al. (2014) mentions that up to seven different types of vortex breakdown states have been observed and that two or more of these states may exist simultaneously. A more quantitative picture of the flowfield would aid in decoding the spray

distribution observed in case 2. Luckily the Swirl-Venturi has been well studied both experimentally and computationally.

In both the work of Fu (2008) and Tedder, et al. (2014) velocity measurements were taken downstream of the Swirl-Venturi Lean Direct Injector with varied swirl number. Fu investigated non-reacting cases with varying air swirler vane angles of 40^0, 45^0, 50^0, 55^0, 60^0 and 65^0. For these cases vortex breakdown transition occurs between the 50 and 55 degree cases. In the 50 degree case, only a very small recirculation is present which is very unstable. The 55 degree case shows a recirculation zone that is lifted above the injector downstream. It was noted that the recirculation zone for the 55 degree case was unstable and moved up and down axially downstream. This instability accounted for the highest amount of axial turbulent intensity at the exit due to this unstable recirculation zone. For the 60 degree case, the recirculation moves upstream and is stable, starting at the exit. The recirculation of the 60 degree case is also stronger in strength than the 55 degree case. Instabilities present in the transition in flow states toward central recirculation may cause an interruption to the air-spray interaction, which assists the primary and secondary breakup of the atomization process, resulting in incomplete primary breakup and higher overall signal at the exit for laser scattering for case 2 of the present work.

Tedder, et al. (2014) investigated the Swirl-Venturi LDI with 45, 52 and 60 degree air swirlers. This study also used a liquid water spray with operating conditions similar to that of Hicks, et al. (2014), air flow rate of 0.107 kg/s and a water flow rate of 3.89 kg/h. Particle Image Velocimetry (PIV) was taken to measure average the velocity of the water spray and is shown in Figure 5.6. The results of mean Mie scattered signal from the present work are shown again in Figure 5.5 to help visually compare with the velocity flowfield results of Tedder (2014). Figures 5.5 and 5.6 match up well in spray pattern with similar spray cone angles.

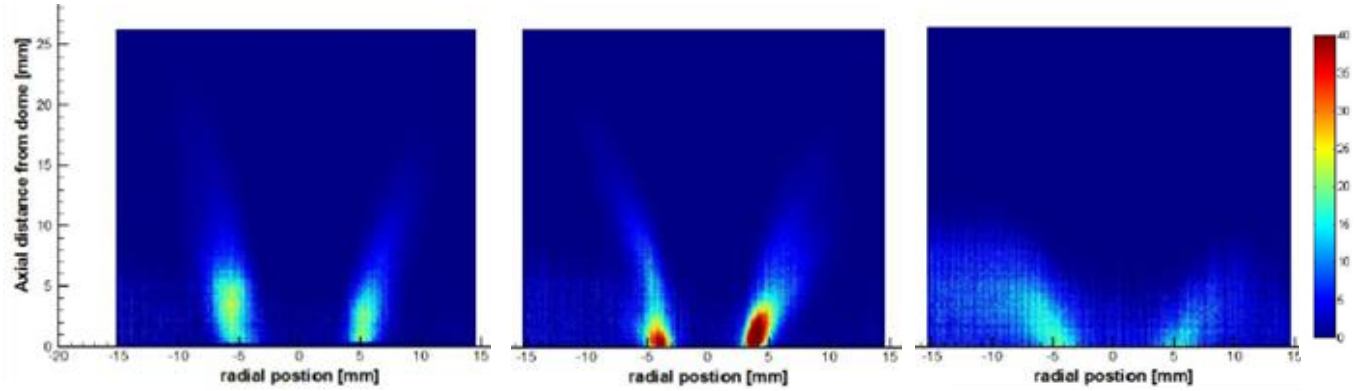

a) b) c)

Figure 5.5 Average Mie Scattering Signal (a) 45 degrees, (b) 52.5 degrees, (c) 60 degrees (The flow is bottom to top)

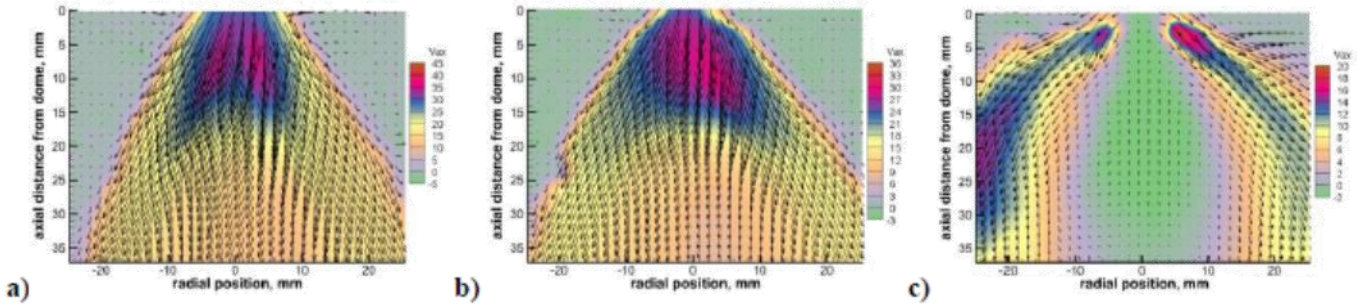

Figure 5.6 Average Velocity Fields (a) 45 degrees, (b) 52.5 degrees, (c) 60 degrees (The flow is top to bottom)

Source: Tedder, et al. 2014

To measure the shape of the spray cone angle in the velocity data of Tedder (2014) a geometric angle was found between two rays which approximately bisected the jets core. The angles measured for Tedder (2014), were 44, 48, and 94 degrees for the 45, 52, and 60 degree air swirler cases respectively. Figure 5.7 shows both the construction of the velocity angle for a 60 degree air swirler case and the plotted comparison of Tedder (2014) and the present work.

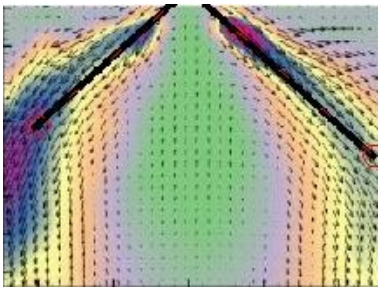

a)

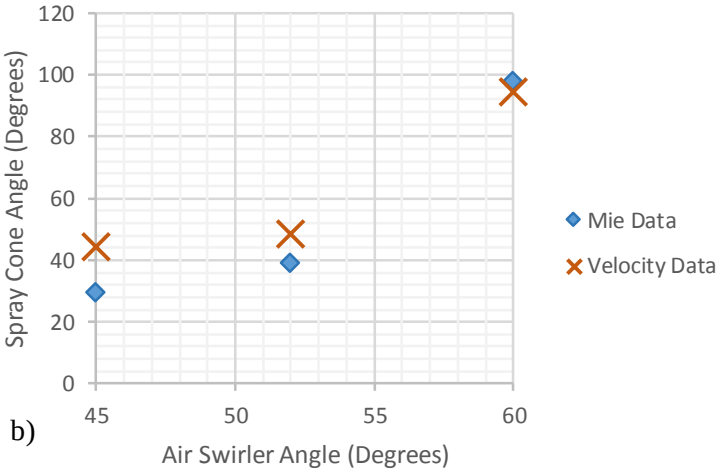

b)

Figure 5.7 Spray Angle Comparision (a) Example of velocity angle with 60 degree air swirler case, (b) Mie data plotted with mean velocity spray cone angles

CHAPTER 6

EFFECT OF MOMENTUM RATIO

In section 6.1 the effects of momentum ratio on the atomization and mixing performance is compared with current literature. In section 6.2, the operating conditions of varying mass flow of air is presented. In section 6.3, the mean statistics of the results are presented. Section 6.4, a discussion of the results is made.

6.1 Effect of Momentum Ratio

This section presents relevant literature to support the results relating to the effects of momentum of air to liquid. (Karnawat and Kushari, 2006) found that changes in the air to liquid ratio can have a large effect on the spray cone angle, solidity, break up distance, and Sauter Mean Diameter (SMD). (Dvorak, et al. 2012), it was mentioned that an important flow condition was the relative momentum and mass flow of liquid to air. In this work many different ALR were taken from 0.2 to 3 with both liquid water and a fuel substitute, using PIV and LDV measurement techniques. The primary parameter of interest was velocity. It is seen that that the results from the two different techniques are not well correlated. It is found that the velocity field depends heavily on the type of fluid used as opposed to the ALR. This was an air blast injector with 30 degree inner and outer air swirlers. The results presented using Mie scattering, and had ALR values ranging from 15 to 36. Similar to that of (Hicks, et al. 2014) which was an ALR of 28.6. The effect of mass loading ratio was conducted by **(**Madsen, 2006) and found that an increase in the mass loading ratio causes an increase in mean axial velocity and a reduction in the SMD.

6.2 Operating Conditions

The results presented were taken at six different operating conditions to observe the effect of liquid to gas momentum ratios on atomization and mixing performance. The six conditions labeled A, B, C, D, E, and F are presented below in Table. 6.1, and for each of these conditions the three swirlers 45, 52, and 60 degree vane angle were tested, giving a total of eighteen test points.

Table 6.1 Operating Conditions

Case	Reynolds Number	Air Velocity	Air mass flow	Liquid mass flow	ALR
A	8,490	6.01 m/s	1.09×10^{-2} kg/s	6.92×10^{-4} kg/s	15.79
B	9,559	6.76 m/s	1.23×10^{-2} kg/s	6.92×10^{-4} kg/s	17.78
C	12,231	8.65 m/s	1.58×10^{-2} kg/s	6.92×10^{-4} kg/s	22.75
D	12,735	9.01 m/s	1.64×10^{-2} kg/s	6.92×10^{-4} kg/s	23.69
E	15,284	10.81 m/s	1.97×10^{-2} kg/s	6.92×10^{-4} kg/s	28.44
F	19,117	13.52 m/s	2.46×10^{-2} kg/s	6.92×10^{-4} kg/s	35.57

6.3 Mean Results

The results of varying momentum ratio are shown in both mean and RMS statistics. These 2-D images provide a qualitative description of spray performance and mixing. Similar to the methods described in the previous results of variation of vane angle, the liquid penetration length, the shape and signal intensity, and the mixing quality will be discussed. For a given air swirler the cases will be labeled A through F with increasing air flow rate, case A being the lowest and F the highest. The first cohort of results to be discussed will be that of a 45 degree vane-angle air swirler

with a swirl number of 0.58. The mass of liquid flowing out of the nozzle will be fixed at 6.92×10^{-4} kg/s and the mass of air will vary from 1.09×10^{-2} kg/s to 2.46×10^{-2} kg/s. To label this cohort Case A1 will denote that it is condition A with swirler number 1, which is a 45 degree air swirler.

The results are discussed in a similar way as section 5.3, showing liquid spray penetration length using methods of threshold of the maximum scattered light intensity. In case A1 with a threshold of 3% the length was approximately 25 mm downstream of the frame. Case B1 the penetration length was 25 mm downstream of the frame. In case C1 the penetration length was 22 mm downstream of the frame at a 3% threshold. Case D1 the penetration length was 21 mm downstream of the frame at a 3% threshold. Case E1 the penetration length was 16 mm downstream of the frame at a 3% threshold. Case F1 the penetration length was 13 mm downstream of the frame at a 3% threshold. As the air flow rate increases from case A1 to F1 the spray penetration length decrease for both large and small drops. More turbulent energy is imparted on the spray aiding in atomization creating finer droplets and bringing the spray lengths upstream toward the injector dome.

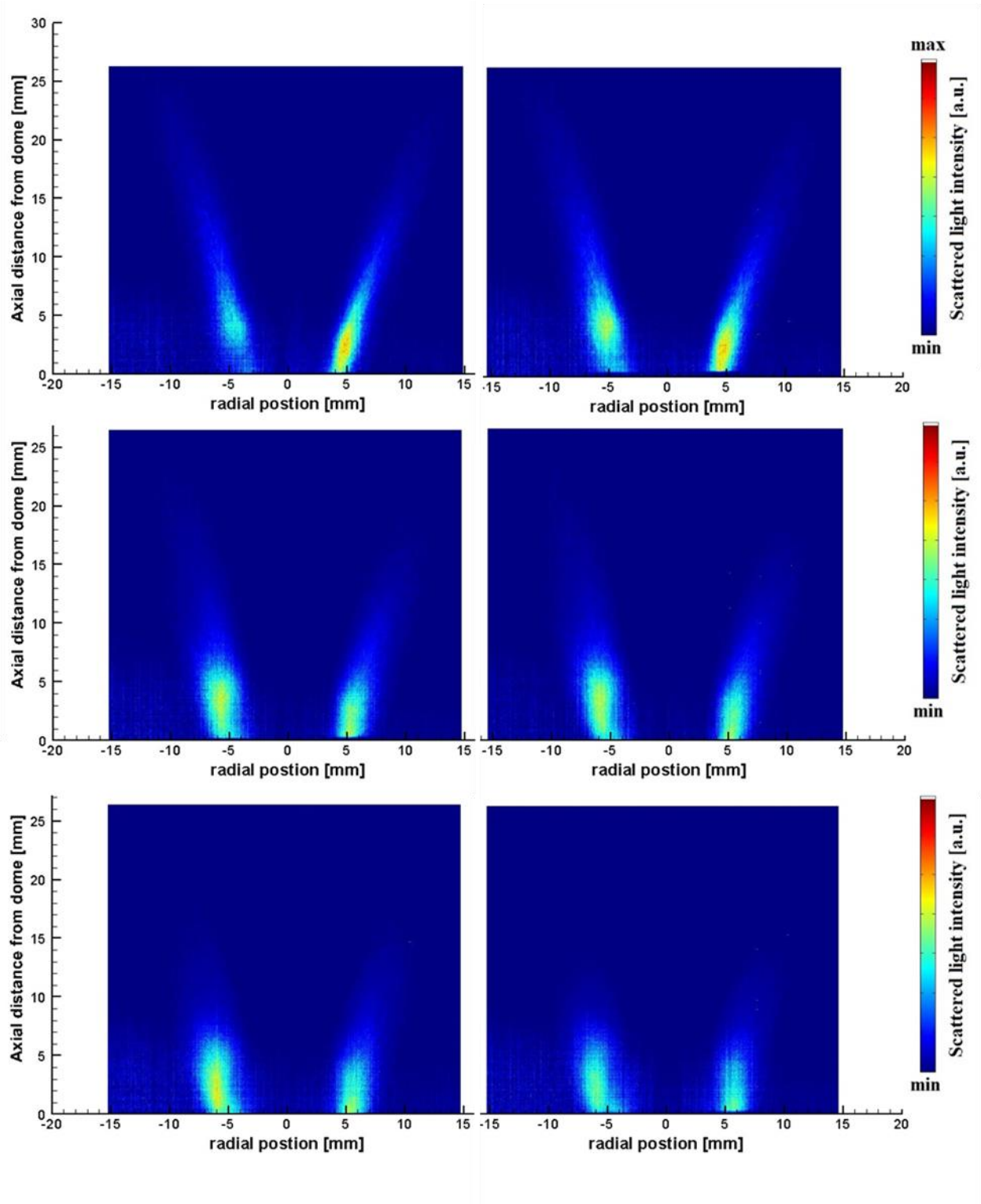

Figure 6.1 Mean results of cases A1-F1

For case A1, the spray is not well dispersed along the cone the spread angle is narrow, along the line of the cone it is not well dispersed. There is noticeable difference in signal intensity at the base of the right lobe to left lobe. From 0 – 5 mm downstream there appears to be an increase of liquid on the right lobe. Case B1 has a better balance of signal intensity between the right and left lobes. Although the right lobe has more intensity than the left. Both right and left lobe widths are wider and more dispersed than case A1. From the results, cases A1 and B1 show a pocket of droplets on the left lobe, this may be a location downstream of secondary breakup of the spray. To investigate this small feature further it would be beneficial to take images at multiple cross plane stations. In case C1, the sheath widths are greater than in case B1. The height of the primary breakup region is lower from 14 mm downstream to 12 mm. The left lobe of the sheath intensity is greater than the right lobe. Case D1 is very similar to C1. In looking at the profiles of signal intensity at a 1 mm axial station the overall signal is greater in case C1 than case D1. In case E1, the spray sheath widths are also wider. There is a slightly higher signal intensity in the left lobe, and the breakup length is shorter. In case F1, the sheath widths are wider than case E1. The overall signal intensity is lower and the spray penetration lengths are shorter.

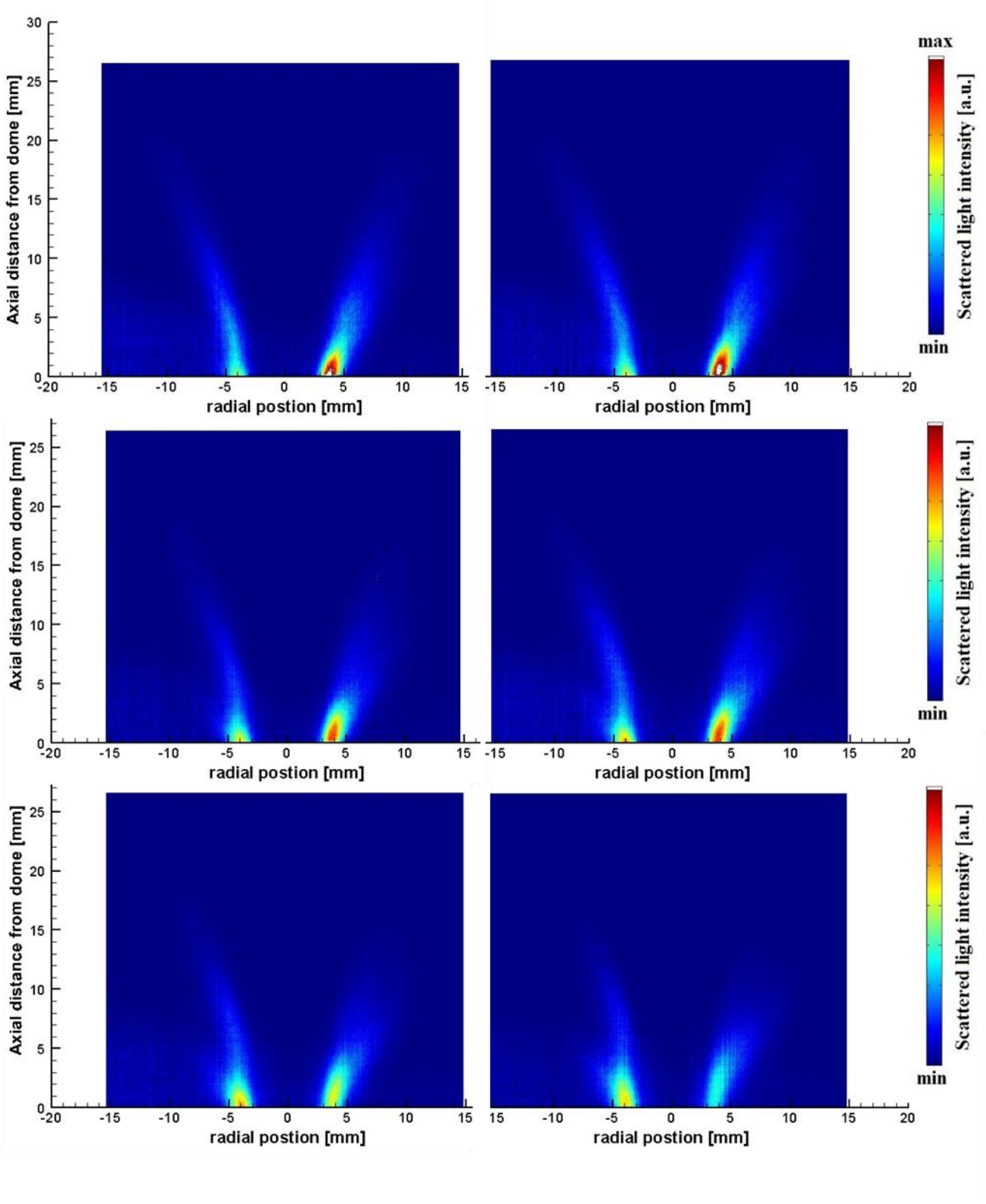

Figure 6.2 Mean results of cases A2-F2

The conditions presented in the set A2-F2 had the same laser power, focal length, exposure, frame rate. This provides the author the abilty to use signal intensity as a meausre of drop size and number density. The results presented in this section are six cases using the same fuel nozzle air swirler combination with a 52 degree CCW air swirler. In case A2 with a threshold of 3% the length was approximately 23 mm downstream of the frame. In case B2, the penetration length was 23 mm downstream of the frame at a 3% threshold. In case C2, the penetration length was 20 mm downstream of the frame at a 3% threshold. For case D2, the penetration length was 21 mm downstream of the frame at a 3% threshold. In case E2, the penetration length was 18 mm downstream of the frame at a 3% threshold. For case F2, the penetration length was 16 mm downstream of the frame at a 3% threshold.

For case A2, the spray has a slight curvature unlike the cases A1-F2 which had fairly straight spray cone sheaths the left lobe of case A2 curves outward with increasing axial distance from the injector dome. The right lobe has a very strong signal at the base of the frame, so much so the signal has saturated. The widths of the right and left lobe are also asymmetric where the left lobe is narrow and slightly curved the right lobe is wider and straighter. In case B2, the same general character as case A2 with slightly curving left lobe and short dispersed right lobe. The intensity of both left and right lobe are slightly greater and the right lobes peak signal has shifted downstream. The signal of the right lobe is still saturating, indication a high amount of liquid at that location. Case C2 has the beginnings of a bifurcation in the spray on the left lobe, a feature that will become more distinct in later cases. This bifurcation feature is not a result of averaging but intrinsic to the instantaneous images taken at this cross plane location. This case has lower overall intensity than that of case B2. The signal intensity is lower at the base right lobe. In case D2, the bifurcation is more evident than C2. The overall intensity is slightly greater with the

effects of C2 shifted upstream approximately 1 mm. In case E2, the overall intensity has dropped and both left and right lobes are more dispersed. The spray topology is shorter and moved upstream from D2. In case F2, the overall intensity has dropped from E2. The left lobe has a greater intensity than the right. The spray shape has moved upstream from E2. Strong signal is present and there is a decrease in jet breakup length as ALR increases. The spray topology is slightly asymmetric with the right lobe with a more dispersed. The left lobe has a bifurcated shape.

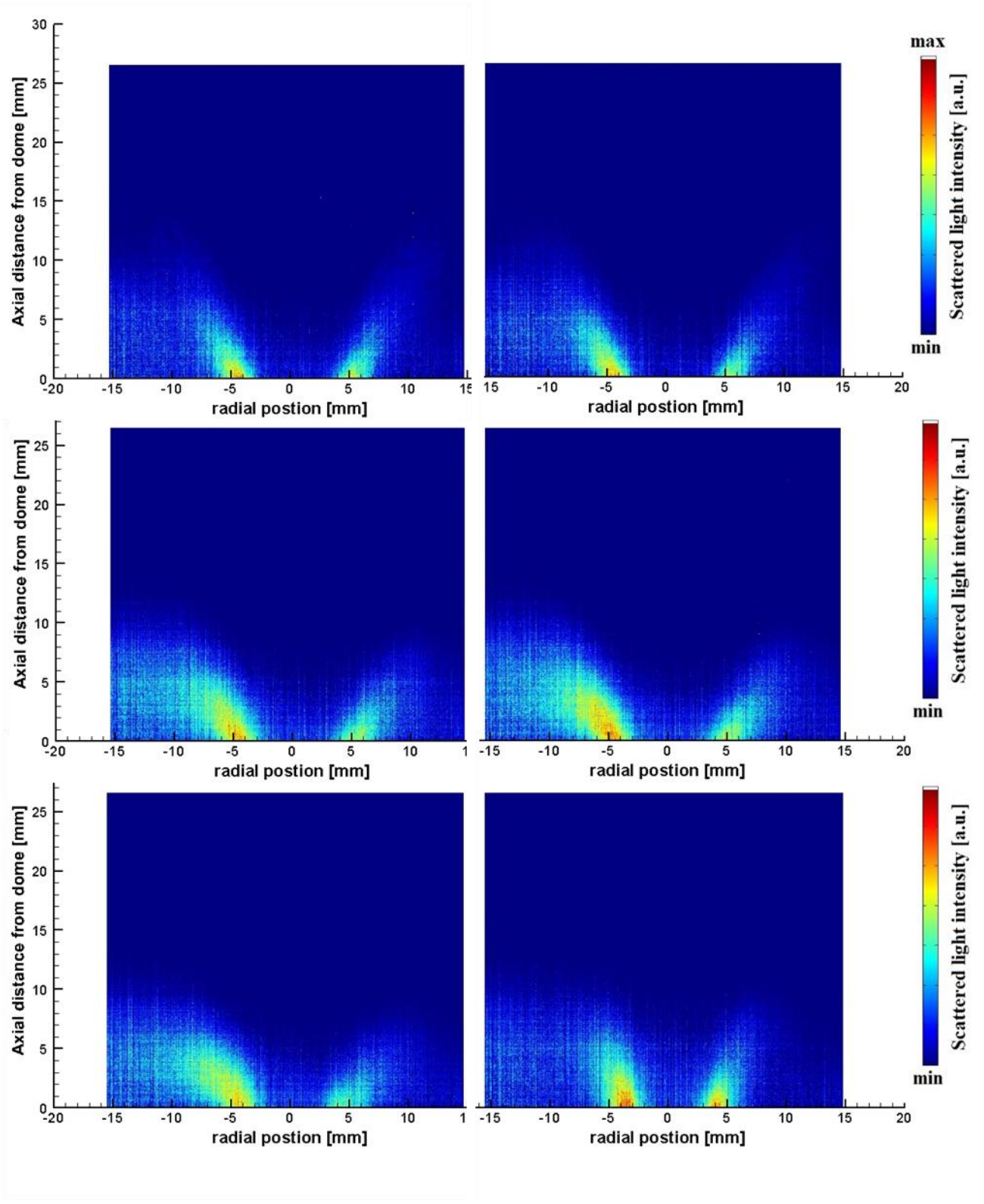

Figure 6.3 Mean results of cases A3-F3

The conditions presented in the set A3-F3 had the same laser power, focal length, exposure, frame rate. This provides the author the abilty to use signal intensity as a meausre of drop size and number density. The results presented in this section are six cases using the same fuel nozzle air swirler combination with a 60 degree CW air swirler. In case A3 with a threshold of 3% the length was approximately 13 mm downstream of the frame. For case B3, the penetration length was 12 mm downstream of the frame. In case C3, the penetration length was 11 mm downstream of the frame at a 3% threshold. For case D3, the penetration length was 12 mm downstream of the frame at a 3% threshold. In case E3, the penetration length was 11 mm downstream of the frame at a 3% threshold. For case F3, the penetration length was 11 mm downstream of the frame at a 3% threshold.

The first noticeable characteristic of this swirler configuration, i.e. for all of cases A3-F3, is the strong dispersion of the spray throughout the lower half of the frame. This strong dispersion is likely due to the nature of flows with higher swirl numbers. Huang and Yang (2005) explain that with higher swirl number brings the effects of vortex breakdown upstream, increased turbulent kinetic energy, and a stronger central recirculation zone. In the results presented it is evident that these effects are present in the flowfield aiding in both atomization and mixing of this set of cases. For case A3, the spray has a pocket of finely dispersed drops in the left part of the frame. The signal intensity at the base of the left lobe is slightly greater than the right lobe. In case B3, the spray has overall greater intensity in the left side of the frame and the left lobe has slightly stronger intensity than that of case A3. Case C3 has more overall signal intensity than B3. The left lobe is also wider and more dispersed. Case D3 has more overall signal intensity than in case C3. Case E3 has less overall signal intensity than in case D3. Case F3 is an interesting case where the spray cone angle changes dramatically. This was an audibly buzzing case and it is likely an aero-acoustic

phenomena which changed the exit conditions of the swirler such that more axial flow was dominant.

6.4 Momentum Ratio Discussion

The momentum ratio of liquid-to-air is an important characteristic for atomization as this is analogous to changing fuel-to-air ratios. The effects of changing fuel-to-air ratios is more notable in the changes to the chemistry of combustion, however the work presented does show change to physical mechanisms of the atomization process. Figure 6.5 shows these changes in spray penetration length with increasing air flow or air-to-liquid mass flow rate ratio (ALR). A decreasing penetration is found with increasing the ALR. This decreasing trend of penetration length is likely due to the increasing interaction between the air flow and the spray assisting in the liquid breakup process and creating a dispersed mix of very small droplets. The trend line for the 60 degree case remains fairly flat as momentum ratio increases. The 45 degree case has the steepest slope of the three cases decreasing most rapidly. The 52 degree case is in between with a slope that is steeper than the 60 degree case but shallower than the 45 degree case. The figure also highlights similarity in spray penetration length of the 45 and 52 degree cases with decreasing momentum ratio. The similar penetration lengths is analogous to the discussion of similar spray cone angles between these two cases. The impact of these observations in changing spray pattern with changing momentum ratio may help validate modeling and predict the location of the flame zone.

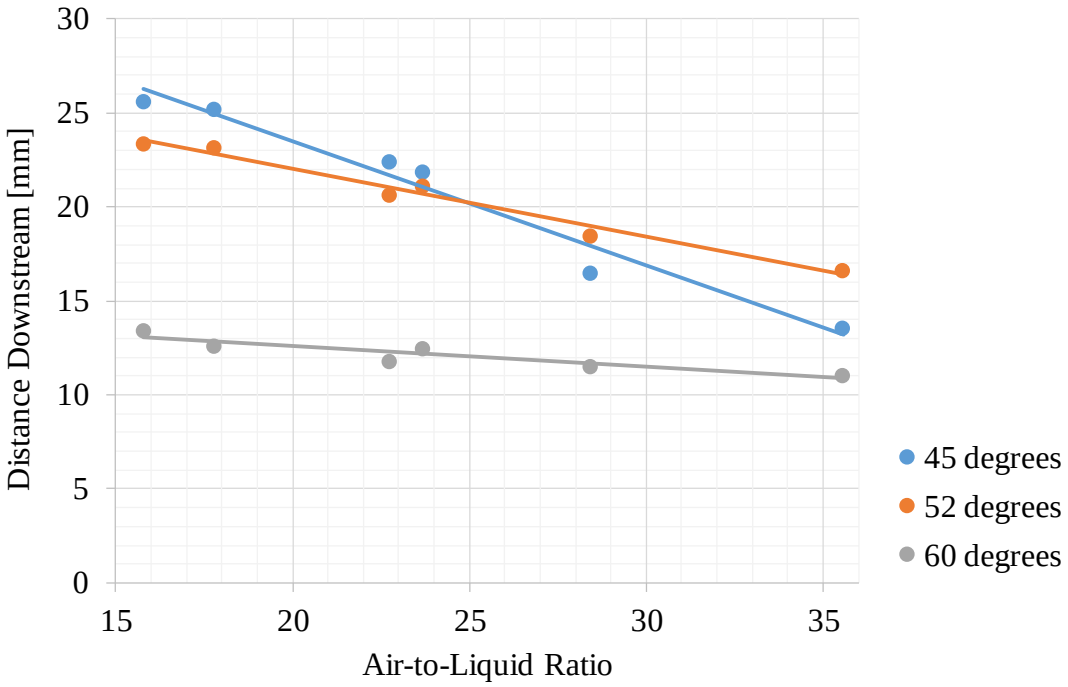

Figure 6.4 Spray Penetration Length Results

CHAPTER 7

DISCUSSION

This paper investigated the effects of swirl number and momentum ratio on the atomization and mixing performance of Swirl-Venturi Lean Direct Injection technology. The spray angle and spray penetration lengths were measured using laser diagnostic techniques. A transition was observed in the liquid spray distribution for the 52 degree case, which unexpectedly produced twice as much signal than the 45 and 60 degree cases. The main cause of this increased signal may be due to instabilities in the flow when transitioning from low to high swirl states. The results from investigation of swirl number it was found that the spray pattern for is sensitive to swirl intensity. Two flow states were observed for a lower and higher swirl flow as well as a transition state that occurred with the lower swirl state. This work may aid in the specific inquiry of physical mechanisms relating to the effect of flow states on spray distribution. It is found that improved atomization and mixing performance are a result of increase in swirl number. As swirl number increases the spray penetration length decreases and spray pattern moves upstream toward the injector. The results from investigation into momentum ratio show decreasing spray penetration length with increasing momentum ratio. The mixedness and dispersion of droplets was found to increase with increasing momentum ratio.

Future work may investigate the effects of flame stability, acoustic perturbation and transition of swirling flows. To access the flame stability reacting cases may offer insights into the tradeoffs of NOx performance and flame stability. The 45 degree case may have better NOx character than that of the 52 and 60 degree air swirlers (Tacina, et al. (2005)), however investigation into the flame stability and operating range of the 45 and 52 degree cases may help in understanding the overall performance of these injectors. Case F3 from the present work had

an audible buzzing and produced a spray cone angle that was half that of the previous case 3. Acoustic perturbations present in aircraft combustors can couple with fluid phenomena altering the flow state and likewise altering the liquid spray distribution, therefore future testing of acoustic forcing of sprays cases may help in understanding mechanisms of aeroacoustics and atomization. Lastly, it may benefit to investigate more cases from swirl numbers 0.6 to 0.8 with combined velocimetry and spray distribution (Mie scattering) to understand greater detail of the air-spray interaction within a transition flow.

REFERENCES

Adam, A., Philippe Leick , Gerd Bittlinger, Christof Schulz, "Visualization of the evaporation of a Diesel spray using combined Mie and Rayleigh scattering techniques," 14th Int Symp on Applications of Laser Techniques to Fluid Mechanics Lisbon, Portugal, 7-10 July, 2008

Anderson, D. N., "Effects of Fuel-Injector Design on Ultra-Lean Combustion Performance," NASA-TM-82624, 1981.

Berrocal, E., Elias Kristensson, Mattias Richter, Mark Linne and Marcus Aldén. "Multiple Scattering Suppression in Planar Laser Imaging of Dense Sprays by Means of Structured Illumination," ILASS 2008 Sep. 8-10, 2008, Como Lake, Italy

Brown, C.T., V.G. McDonell, D.G. Talley. "Accounting for Laser Extinction, Signal Attenuation, and Secondary Emission While Performing Optical Patternation in a Single Plane," Fifteenth Annual Conference on Liquid Atomization and Spray Systems, Madison, WI, USA, May 2002.

Cai, J., S.-M. Jeng, R. Tacina. "Multi-Swirler Aerodynamics: Comparison of Different Configurations," Proceedings of ASME Turbo Expo 2002 June 3-6, 2002, Amsterdam, the Netherlands.

Chang, C.T., Lee CM, Herbon JT, Kramer SK, "NASA Environmentally Responsible Aviation Project Develops Next-Generation Low-Emissions Combustor Technologies (Phase I)". J Aeronaut Aerospace Eng 2: 116. 2013.

Charalampous, G., and Y.Hardalupas. "Comparison between signal attenuation correction methodology for LIF and scattered light intensity measurements in dense sprays," 17th International Symposium on applications of Laser Techniques to Fluid Mechanics Lisbon, Portugal, 07-10 July, 2014.

Chryssakis, C., Assanis, D., Lee, J., and Nishida, K., "Fuel Spray Simulation of High-Pressure Swirl-Injector for DISI Engines and Comparison with Laser Diagnostic Measurements," SAE Technical Paper 2003-01-0007, 2003.

Cooper, C. S., and N.M. Laurendeau "Quantitative Measurements of Nitric Oxide Concentration in High-Pressure, Swirl-Stabilized Spray Flames," NASA/CR-2000-210365

Dewanji, D., "Flow Characteristics in Lean Direct Injection Combustors," PhD thesis, Technische Universiteit Delft, 2012.

Doerr, Th., "The Significance of Fuel Preparation for Low Emissions Aero-Engine Combustion Technnology" ICLASS 2012, 12th Triennial International Conference on Liquid Atomization and Spray Systems, Heidelberg, Germany, September 2-6, 2012

Dunn-Rankin (ed) Lean Combustion: Technology and Control, Academic Press, 2008.

Dvorak, D., Spencer Pack, and Hui Hu "An Experimental Investigation on the Spray Flows Exhausted from a Co-swirling Air-blast Nozzle," 28th Aerodynamic Measurement Technology,Ground Testing, and Flight Testing Conference 25 - 28 June 2012, New Orleans, Louisiana

Emadi, M., "Flame structure and thermo-acoustic coupling for the low swirl burner for elevated pressure and syngas conditions," PhD thesis, University of Iowa, 2012

Falese, M., L.Y.M. Gicquel, and T. Poinsot, "LES of bifurcation and hysteresis in confined annular swirling flows" Computers & Fluids 89. 2014. pp. 167–178.

Feikema, D., Ruey-Hung Chen, and James F. Driscoll "Enhancement of Flame Blowout Limits by the Use of Swirl," Combustion and Flame 80. 1990. pp. 183-195.

Fink, R., "Studies on LPP aircraft engine combustion chambers under elevated pressure", Ph. D. thesis, Technische Universität München, 2001.

Fu, Y., "Aerodynamics and Combustion of Axial Swirlers," PhD thesis, University of Cincinnati, 2008.

Glassman, I. and Yetter, R.A. (eds), Combustion. Academic Press. 2008.

Goeke, J., S. Pack, G. Zink, and J. Ryon "Multi-Point Combustion System," NASA/CR-218112, 2014

Hicks, Y.R., DeGroot, W.A., Locke, R.J., Anderson, R.C. "Combustion Temperature Measurement by Spontaneous Raman Scattering in a Jet-A Fueled Gas Turbine Combustor Sector," NASA/TM-211588, 2002.

Hicks, Y.R., and K.M. Tacina "Comparing a Fischer-Tropsch Alternate Fuel to JP–8 and Their 50-50 Blend: Flow and Flame Visualization Results," NASA/TM-217884, 2013.

Hicks, Y.R., S.A. Tedder, K.M. Tacina and R.C. Anderson "Fundamental study of a single point lean direct injector. Part II: a comparison of cold flow and burning measurements," Spring Technical Meeting of the Central States Section of the Combustion Institute Mar 16–18, 2014

Huang, Y., and V. Yang "Effect of swirl on combustion dynamics in a lean-premixed swirl-stabilized combustor," Proceedings of the Combustion Institute, 30. 2005. pp. 1775–1782

Huang, Y., "Combustion dynamics of swirl-stabilized lean premixed flames in an acoustically-driven environment," PhD thesis, University of Iowa, 2008.

Iannetti, A.C., N.-S. Liu, F. Davoudzadeh "The Effect of Spray Initial Conditions on Heat Release and Emissions in LDI CFD Calculations," NASA/TM-215422, 2008.

Johnson, S.M., "Venturi nozzle effects on fuel drop size and nitrogen oxide emissions," NASA-TP-2028, 1982.

Karkow, D., "Combustion instabilities: an experimental investigation on the effects of hydrogen in a lean premixed combustor," PhD thesis, University of Iowa, 2012.

Karnawat, J., and Kushari A "Controlled atomization using a twin-fluid swirl atomizer," Exp Fluids, Vol. 41, August 2006, pp.649-663.

Kaufman, K., "Effect of hydrogen addition and burner diameter on the stability and structure of lean, premixed flames," PhD thesis, University of Iowa, 2014.

Khavkin, Y.I., Theory and Practice of Swirl Atomizers, CRC Press, 2003

Knudsen, E., and H. Pitsch "Large eddy simulation of a spray combustor using a multi-regime flamelet approach," Center for Turbulence Research Annual Research Briefs, 2010. pp. 337-350

Lefebvre, A.H., Atomization and Sprays, CRC Press, 1988

Liang, H., and T. Maxworthy, "An experimental investigation of swirling jets," J. Fluid Mech. vol. 525, 2005. pp. 115–159

Lieuwen, T.C. and Yang, V.(eds), Combustion Instabilities in Gas Turbine Engines: Operational Experience, Fundamental Mechanisms, and Modeling, AIAA Progress in Astronautics and Aeronautics, Vol. 210, 2005.

Locke, R. J., Y. R. Hicks, R. C. Anderson, M. M. Zaller, "Optical Fuel Injector Patternation Measurements in Advanced Liquid-Fueled, High Pressure, GasTurbine Combustors," Combustion Science and Technology, 138:1-6, pp. 297-311

Mansour, A., "Gas Turbine Fuel Injection Technology," Paper 2005-GT-68173, ASME: Turbo Expo 2005, Reno-Tahoe, Nevada, USA.

Madsen, J., "Computational and Experimental Study of Sprays from the Breakup of Water Sheets," PhD thesis, Aalborg University, 2006.

Marek, C., Timothy D. Smith, and Krishna Kundu, "Low Emission Hydrogen Combustors for Gas Turbines Using Lean Direct Injection," 41st AIAA/ASME/SAE/ASEE Joint Propulsion Conference and Exhibit AIAA–2005–3776. Tucson, Arizona, July 10–13, 2005

McKinney, R.G., D. Sepulveda, W. Sowa, A.K. Cheung, "The Pratt &Whitney TALON X Low Emissions Combustor: Revolutionary Results with Evolutionary Technology," 45th AIAA Aerospace Sciences Meeting and Exhibit 8 - 11 January 2007, Reno, Nevada

Mishra, Y. N., E. Kristensson, and E. Berrocal, "Reliable LIF/Mie droplet sizing in sprays using structured laser illumination planar imaging," Optics Express, Vol. 22, Issue 4, 2014. pp. 4480-4492

Ng, L.N. "Manipulation of Particles on Optical Waveguides," PhD thesis, University of Southampton, 2000, pp. 23-61

Patel, N., and S. Menon, "Simulation of spray–turbulence–flame interactions in a lean direct injection combustor," Combustion and Flame, 153, 2008, pp. 228–257

Schmidt, J., "Qualitative measurements of pressure-atomized sprays through simultaneous collection of planar fluorescence, phosphorescence, and Mie scattering data", PhD thesis, Iowa State University, 2009.

Siebers, D.L., "Liquid-phase fuel penetration in diesel sprays" SAE Paper 980809. 1998.

Sturgess, G. J., J. Zelina, D.T. Shouse, and W. M. Roquemore, "Emissions Reduction Technologies for Military Gas Turbine Engines," JPP Vol. 21, No. 2, March–April 2005. pp. 194-217

Syred, N., and J.M. Beer, "Combustion in Swirling Flows: A Review," Combustion and Flame 23. 1974, pp. 143-201

Tacina, K.M., C.-M. Lee, C. Wey, "NASA Glenn High Pressure Low Nox Emissions Research," NASA/TM-214974, 2008.

Tacina, K.M., "Swirl-Venturi Lean Direct Injection Combustion Technology," Spring Technical Meeting of the Central States Section of the Combustion Institute April 22–24, 2012

Tacina, R. R., "Degree of Vaporization Using an Airblast Type Injector for a Premixed-Prevaporized Combustor," NASA TM-78836, 1978.

Tacina, R. R., "Combustor technology for future aircraft," NASA-TM-103268, 1990

Tacina, R. R., C.-P. Mao, C. Wey,"Experimental Investigation of a Multiplex Fuel Injector Module for Low Emission Combustors" 41st Aerospace Sciences Meeting and Exhibit 6-9 January 2003, Reno, Nevada

Tacina, R. R., C.-P. Mao, C. Wey, "Experimental Investigation of a Multiplex Fuel Injector Module with Discrete Jet Swirlers for Low Emission Combustors," NASA/TM-212918, 2004.

Tacina, R. R., L., Phil, and W., Changlie, A lean-direct-injection combustor using a 9 point swirl-venturi fuel injector, ISABE-2005-1106, 2005.

Tedder, S., Y.R. Hicks, K.M. Tacina, and R.C. Anderson, "Fundamental study of a single point lean direct injector. Part I: effect of air swirler angle and injector tip location on spray characteristics" 50th AIAA/ASME/SAE/ASEE Joint Propulsion Conference. AIAA 2014-3435. July 28-30, 2014, Cleveland, OH.

Turns, S.R., An introduction to Combustion, Mcgraw Hill, 2000.

Vanierschot, M., and E. Van den Bulck, "Hysteresis in flow patterns in annular swirling jets" Experimental Thermal and Fluid Science. 31. 2007. pp. 513–524.

Wellander, R., E. Berrocal, E. Kristensson, M. Richter and M. Aldén, "Three-dimensional measurement of the local extinction coefficient in a dense spray," Meas. Sci. Technol. 22 125303. 2011

Yoon, C., Gejji, R., Anderson, W. and Sankaran, V., "Computational Investigation of Combustion Dynamics in a Lean-Direct Injection Gas Turbine Combustor," 51st AIAA Aerospace Sciences Meeting, Dallas, Texas, 7-10 January 2013

Yushanov, S., J.S. Crompton, and K.C. Koppenhoefer, "Mie Scattering of Electromagnetic Waves," Proceedings of the COMSOL Conference, Boston, 2013.